

SANDIA REPORT

SAND98-2716

Unlimited Release

Printed December 1998

Relativistically Self-Channeled Femtosecond Terawatt Lasers for High-Field Physics and X-Ray Generation

Stewart M. Cameron, Ting Shan Luk, Alex B. Borisov, Keith Boyer, Armon McPherson,
Tom Nelson, and Charles K. Rhodes

Prepared by
Sandia National Laboratories
Albuquerque, New Mexico 87185 and Livermore, California 94550

Sandia is a multiprogram laboratory operated by Sandia Corporation,
a Lockheed Martin Company, for the United States Department of
Energy under Contract DE-AC04-94AL85000.

Approved for public release; further dissemination unlimited.



Sandia National Laboratories

Issued by Sandia National Laboratories, operated for the United States Department of Energy by Sandia Corporation.

NOTICE: This report was prepared as an account of work sponsored by an agency of the United States Government. Neither the United States Government nor any agency thereof, nor any of their employees, nor any of their contractors, subcontractors, or their employees, makes any warranty, express or implied, or assumes any legal liability or responsibility for the accuracy, completeness, or usefulness of any information, apparatus, product, or process disclosed, or represents that its use would not infringe privately owned rights. Reference herein to any specific commercial product, process, or service by trade name, trademark, manufacturer, or otherwise, does not necessarily constitute or imply its endorsement, recommendation, or favoring by the United States Government, any agency thereof, or any of their contractors or subcontractors. The views and opinions expressed herein do not necessarily state or reflect those of the United States Government, any agency thereof, or any of their contractors.

Printed in the United States of America. This report has been reproduced directly from the best available copy.

Available to DOE and DOE contractors from
Office of Scientific and Technical Information
P.O. Box 62
Oak Ridge, TN 37831

Prices available from (615) 576-8401, FTS 626-8401

Available to the public from
National Technical Information Service
U.S. Department of Commerce
5285 Port Royal Rd
Springfield, VA 22161

NTIS price codes
Printed copy: A03
Microfiche copy: A01



SAND 98-2716
Unlimited Release
Printed December 1998

Relativistically Self-Channeled Femtosecond Terawatt Lasers for High-Field Physics and X-Ray Generation¹

S.M. Cameron* and T.S. Luk
Pulsed Power and Laser Initiatives Department
Sandia National Laboratories, P.O. Box 5800, Albuquerque NM 87185-1188

A.B. Borisov, K. Boyer, A. McPherson, T. Nelson, and C.K. Rhodes
Dept. of Physics, University of Illinois, Chicago IL 60607

Abstract

Optical channeling or refractive guiding processes involving the nonlinear interaction of intense femtosecond optical pulses with matter in the self-focussing regime has created exciting opportunities for next-generation laser plasma-based x-ray sources and directed energy applications. This fundamentally new form of extended paraxial electromagnetic propagation in nonlinear dispersive media such as underdense plasma is attributed to the interplay between normal optical diffraction and intensity-dependent nonlinear focussing and refraction contributions in the dielectric response. Superposition of these mechanisms on the intrinsic index profile acts to confine the propagating energy in a dynamic self-guiding longitudinal waveguide structure which is stable for power transmission and robust compression. The laser-driven channels are hypothesized to support a degree of solitonic transport behavior, simultaneously stable in the space and time domains (group velocity dispersion balances self-phase modulation), and are believed to be self-compensating for diffraction and dispersion over many Rayleigh lengths in contrast with the defining characteristics of conventional diffractive imaging and beamforming. By combining concentrated power deposition with well-ordered spatial localization, this phenomena will also create new possibilities for production and regulation of physical interactions, including electron beams, enhanced material coupling, and self-modulated plasma wakefields, over extended gain distances with unprecedented energy densities. Harmonious combination of short-pulse x-ray production with plasma channeling resulting from a relativistic charge displacement nonlinearity mechanism in the terawatt regime (10^{18} W/cm²) has been shown to generate high-field conditions conducive to efficient multi-kilovolt x-ray amplification and peak spectral brightness. Channeled optical propagation with intense short-pulse lasers is expected to impact several critical mission areas at Sandia including x-ray backlighting of pinch implosions, nondestructive radiographic imaging of aging weapons components, high-power electromagnetic pulse generation, particle acceleration, and remote sensing.

Keywords: *relativistic self-focussing, chirped-pulse amplification, nonlinear laser-plasma interactions, laser filamentation, "hollow atoms," x-ray backlighting, radiography*

* principal investigator to whom correspondence should be addressed
tel: (505)844-4964; fax: (505)845-7890; e-mail: smcamer@sandia.gov

¹ SAND report in support of LDRD project entitled "Self-Stabilizing Optical Solitons and High-Intensity Plasma Channels for Diffraction-Free Propagation and Robust Power Compression."

Acknowledgement

This work was supported by Divison 9000 discretionary LDRD funds, proposal 99-0836, within the Department of Energy under Contract No. DE-AC04-94AL85000.

Contents

I. Introduction p. 7-10
II. Technical Approach	
- Short-Pulse Laser Plasma Interactions p. 10-15
- Relativistic Self-Channeling p. 15-20
- Anomalous Coupling Physics p. 20-21
III. Experimental Accomplishments	
- Laser System p. 21-23
- X-Ray Spectra p. 23-25
- Diagnosis of Relativistic Channelingp. 25-26,27,28
- X-Ray Calibrationp. 26,29
- Modelling Effortsp. 26-30
IV. Applications	
- X-Ray Backlighting/Radiography p. 30-32
- Ultrafast Probing of Atomic Structure p. 31,33
- Laser Wakefield Accelerator p. 33-34
- Optically-Induced Nuclear Fission p. 34
- Fast Ignitor p. 34-35
- Adaptive Optics p. 35
- Recombination X-Ray Lasers p. 35
- Electromagnetic Pulsesp. 35-36
V. Conclusion p. 36
VI. References p. 37

Figures:

#	Caption	
1	Schematic of electron density and temperature profiles	13
2	Interaction configuration for resonance absorption	13
3	Repeated multi-foci refractive guiding structure	16
4	Morphology of the laser-driven channeling process	18
5	Experimental optimization strategy for next-generation ultrabright x-ray sources	19
6	Feynman representation of enhanced multi-electron coupling	21
7	Spatially resolved (Z - λ) imaging of Xe(L) emission spectrum	22
8	Ultraviolet sub-picosecond terawatt laser design	23
9	L-shell emission spectrum from Au target excited by high-intensity, short-pulse laser	24
10	X-ray yield measurement >20 keV for tantalum thin foil	25
11	Transverse image of Thomson scattering from a self-channeled laser filament	27
12	Pinhole image of Xe(M) ~ 1 keV radiation from a laser channel in gaseous $(Xe)_n$	28
13	Time-dependent x-ray response signals for XRD and PCD devices	29
14	Stability map for relativistic and charge displacement self-channeling	29
15	Spectral intensity of a scaled femtosecond x-ray backlighter	32
16	X-ray optical arrangements for diffractometry and absorption spectroscopy	33

Tables

1	Laboratory-scaleable parameter space for self-focussed femtosecond terawatt lasers	9
---	--	---

Relativistically Self-Channeled Femtosecond Terawatt Lasers for High-Field Physics and X-Ray Generation

I. Introduction

The advent of chirped pulse amplification, broadband dispersion control, and adaptive pulse shaping techniques during the last decade has facilitated the development of laboratory-scale subpicosecond terawatt lasers with focal irradiances approaching 10^{20} W/cm² which can create novel interaction conditions for the production and regulation of many energetic processes including hard x-ray generation, initiation of nuclear reactions, fast ignition of fusion targets, and high-gradient particle acceleration. In this new regime for intense ultrafast laser-matter interactions, extremely rapid ionization of heavy atoms will occur by field emission during a fraction of a laser cycle producing free electron densities at least an order of magnitude larger than in metallic conductors. Because of the short interaction time, hydrodynamic flow and ionic motion associated with the rarefaction wave from the heated target surface are negligible (~ 100 A^o), and the ions form an immobile overdense neutralizing background for the perturbed electronic distribution. The disparity of timescales provides a unique opportunity to study direct coupling of the incident laser field with an vacuum-solid interface discontinuity over a density gradient scalelength ∇n_e less than an optical wavelength λ_{opt} without the complications of coronal preheat or long-range parametric instabilities. Additionally, the presence of a high-intensity laser distribution will also significantly modify the basic constitutive properties of the dense plasma from the classical fluid description, instead producing nonlocal currents and non-Maxwellian internal energy equilibria essentially controlled by the electron quiver velocity v_{osc} in the external driving laser field. When the quiver velocity proportional to $I\lambda^2$ considerably exceeds the electron thermal velocity v_{te} , efficient light absorption and hot electron production occurs by collisionless collective mechanisms near the critical surface such as resonance absorption and vacuum heating rather than by inverse bremsstrahlung as in the case of long scalelength plasma formed by nanosecond pulses.

At the intensities available with terawatt-class short-pulse lasers, the pondermotive energy becomes comparable to the electron thermal energy ($mv_{osc}^2/2 \sim kT_e$), so that kinetic effects can combine with radiation pressure dominated hydrodynamics to form a complex scenario for extremely nonlinear physics. Under these conditions, the light pressure (typically Gbars) can exceed the thermal expansion pressure thereby perturbing the plasma density profile inward to produce strongly-coupled conditions or to initiate pondermotive hole-boring and profile modification (pondermotive steepening) which have important implications for deposition of laser energy at solid density. By using the pondermotive force of the laser to impart momentum to the critical surface and impede expansion, it is possible to accelerate surface ions reactively and to snowplow plasma densities to values greater than the original solid density. Rapid ionization and the strong dependence of the electron-ion collision frequency on quiver velocity will also contribute to a nonlinear refractive index which allows enhanced transparency to non-evanescent optical propagation beyond the critical surface. For a normalized laser field amplitude ($a_0 = \gamma v_{osc}/c$) greater than unity ($eE_0/m_e\omega_0 c > 1$) with $\gamma = (1+a_0^2)^{1/2}$, the cycle-averaged quiver energy of free electrons approaches ~ 100 keV requiring relativistic correction to basic plasma parameters. At these relativistic laser intensities, the transient pulse envelope reaches a substantial fraction of the atomic Coulombic field and the driving laser field can significantly alter the shape of the binding potential. The relativistic focussing effect which leads to an increase in electron mass proportional to γ will reduce the effective electron plasma frequency $\omega_{pe} = (4\pi n_e e^2/m_e)^{1/2}$ below the laser frequency modifying

the dispersion relation $kc=(\omega_{pe}^2/\gamma-\omega_o^2)^{1/2}$ so that anomalous penetration into the classically overdense plasma region can occur. This marked deviation from the nonrelativistic (low-intensity) case results from the increased electron inertia which makes it more difficult to generate the plasma current responsible for reflecting light.

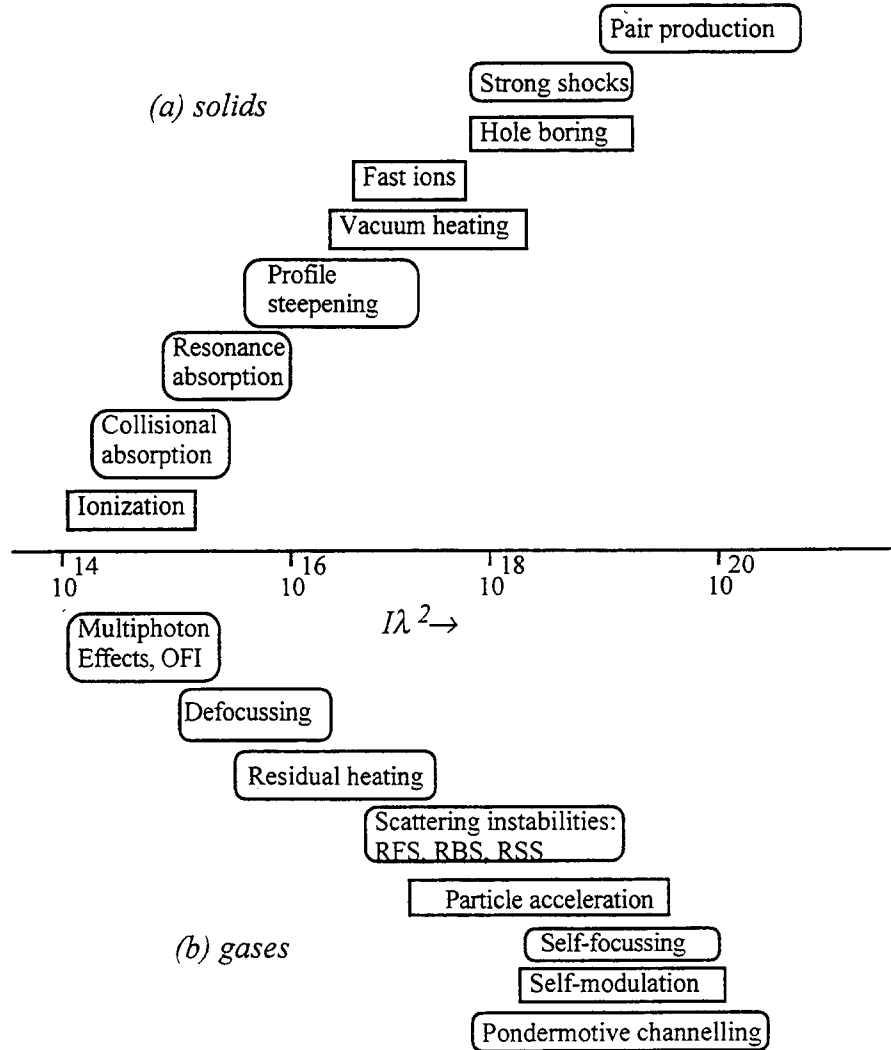
Realization of power compression of intense short-pulses for high-field physical interactions and x-ray generation will require self-sustaining plasma guiding structures which are stable in the presence of strong ionization of dense gases, relativistic self-focussing, and pondermotive charge displacement. The confluence of high-intensity modes of channeled propagation with short-pulse x-ray production will establish exceptional laser-matter conditions for a new class of nonlinear optics experiments. New refractive self-guiding processes involving the nonlinear relativistic interaction of intense ultrafast optical pulses with matter in the self-focussing regime can produce vigorous thermonuclear power densities $\sim 10^{19}$ W/cm³, (1-10 W/atom) over controllable interaction lengths exceeding many confocal Rayleigh lengths. The key to the production of these exceptional conditions is the stable compression and confinement of the spatial distribution of incident pulses of radiation into a narrow longitudinal plasma channel or dynamical waveguide which is compensated for diffractive divergence by virtue of self-induced regularization of the intrinsic refractive index profile. This fundamentally new form of extended paraxial electromagnetic propagation in a nonlinear dispersive medium such as underdense plasma is attributed to a complex interactive mechanism which is triggered by optical pulses whose power exceeds a critical level and involves the superposition of both relativistic electron quiver motion and radial charge displacement caused by radiation pressure of the intense (driving) external wave. Specifically, pondermotive expulsion of electrons and the contrasting inertial confinement of the ions cooperate to produce the chief characteristics of channel formation: (i) the refractive self-focusing action of the displaced electrons which confine the propagating radiation; and (ii) the stability of the channel for robust power transmission due to the immobile electrostatic spine formed by stationary ions which establish force balance. As a consequence of the unprecedented power deposition inherent to the spatio-temporal dynamics of the channel creation process, a new largely unexplored class of strongly nonequilibrium excited matter combining concentrated energy density with well-ordered spatial gain structure can be created which embodies high-field conditions conducive to significant power compression and multi-keV x-ray amplification.

Harmonious use of this nonlinear phenomenon under optimized conditions is expected to lead to an advanced generation of extraordinarily bright x-ray sources and backlighters having a peak spectral brightness $>10^{31}$ ph s⁻¹ mrad⁻² (.1% bandwidth)⁻¹. In addition, spatial organization interior to the trapped focussing state opens a new strong-coupling regime for enhanced laser-atom interactions in which field strengths in the 10-50 (e/a_o^2) range can be selectively applied to promote long-range ordered multi-electron motion and anomalous inner-shell excitation of inverted "hollow atom" electronic configurations for maximum x-ray radiative transition rates and recombination. Furthermore, these field strengths can be developed in a very fast risetime (1-3 fs) less than an optical cycle since the channel formation memory is of order the plasma electron equilibration time $2\pi/\omega_{pe}$. The combination of peak intensity with short interaction time and abrupt time-development profile (no prepulse) of the ionizing electric field amplitude will have profound consequences for material rectification, ionization equilibria, and evolution of the nonsteady-state dielectric response. Efficient stripping of electrons in the presence of an intense laser field to form a dense nonequilibrium plasma will result in a brief population inversion which may facilitate stimulated emission of short-wavelength x-rays.

Whether the target medium placed at focus is gaseous or solid, short-pulse high-intensity interaction with matter generally involves a number of fundamental physical processes: ionization, propagation and refraction, generation of plasma waves, and subsequent thermal and hydrodynamic evolution of target material. These processes sensitively depend upon operative laser parameters, and the impending escalation of laser technology towards shorter pulses and higher intensities has shifted contemporary research emphasis from conventional atomic physics and linear laser-plasma wave interactions to extremely nonlinear collective phenomena. On the application side, this evolution has meant a shift to harder, brighter x-ray sources and production of more energetic particles. The overall organization and content of this report reflects strong advocacy for this technical direction by the authors. In section II, we first present a brief review of the fundamental physical concepts that play a dominant role in intense short-pulse laser interactions including absorption mechanisms, thermal transport, hydrodynamics, relativistic self-focussing, pondermotive channeling, and x-ray generation. Section III describes recent pertinent experimental results conducted with an ultraviolet femtosecond terawatt laser system in collaboration with the University of Illinois-Chicago to characterize relativistic self-channeling and optimize the resulting hard x-ray production from high-Z targets. A number of potential applications of this technology which impact critical mission areas at Sandia such as x-ray backlighting/radiography, material coupling, advanced fusion schemes, recombination lasers, and particle accelerators are described in section IV with an indication of future research problems to be addressed. Published references relevant to a comprehensive understanding this work are listed in the Bibliography section V. Salient features of the new physics regime accessible with ultra-intense channeled lasers are summarized in table 1.

<ul style="list-style-type: none"> • pulse duration < 10 fs (no prepulse) 	negligible hydrodynamics/thermal diffusion near-solid density (10^{23} cm $^{-3}$) gradient scalelength $\nabla n_e < \lambda_{opt}$ rapid ionization
<ul style="list-style-type: none"> • power density $\sim 10^{19}$ W/cm3 	thermonuclear regime $\rightarrow 1-10$ W/atom $\sim 94\%$ coupling into a $5 \mu\text{m}$ ϕ channel collective multi-electron coupling $Z^2\alpha$
<ul style="list-style-type: none"> • focussable intensity $> 10^{20}$ W/cm2 	electric field $> 10^{12}$ V/m magnetic field $> 10^8$ Gauss light pressure $\nabla^2 E > 10$ Gbar self-focussing/charge displacement relativistic currents produced energetic x-rays and hot electrons
<ul style="list-style-type: none"> • energy density $\sim 10^{10}$ J/cm3 	corresponds to 10 keV blackbody

Table 1: Self-focussed femtosecond terawatt lasers will expand laboratory-scaleable parameter space for studying energetic processes. Adjoining diagram indicates the hierarchy of physical phenomena in short-pulse laser interaction with (a) solids and (b) gases as a function of normalized laser intensity $I\lambda^2$. (from Gibbon and Forster)



II. Technical Approach:

• Short-Pulse Laser Plasma Interactions

Plasmas created by intense subpicosecond optical pulses ($I\lambda^2=10^{15-18}\text{W}/\text{cm}^2\mu\text{m}^2$) interacting with solid targets have received considerable attention as novel sources of x-ray radiation. Because the laser drive deposits its energy impulsively over a short scalelength ($\sim 100 \text{ \AA} \ll \lambda_{\text{opt}}$) of near solid-density material on a timescale exhibiting negligible hydrodynamics, the resulting plasma is kinetically cold with highly nonthermal distributions and steep density gradients. These extreme conditions of temperature and electron density cause the atomic processes of ionization, recombination, and collisional excitation and deactivation to occur proportionately faster than hydrodynamic expansion $\sim 100\text{ps}$. The resulting decoupling of timescales for the case of thermal emission from rapidly heated solids makes ultrafast laser-material interactions ideal for the generation of bright x-ray sources. The near solid density of the emitting plasma provides a large number of emitters for photon output, and fast duration of the resulting emission pulse gives high brightness and temporal resolution. Small source size defined by the laser focal region reduces penumbral blurring for image projection.

The observed emission includes coherent radiation at high harmonics of the laser frequency, incoherent K,L,M-shell x-ray thermal emission <20 keV, energetic suprathermal electrons ($T_H > 100$ KeV), prompt quasi-monochromatic K_α fluorescence, and generation of hard nonthermal bremsstrahlung x-rays with typical photon energies extending beyond 1 MeV. Hot electrons are created during nonlinear interaction of the laser field with the plasma by a mixture of tunneling ionization, collisional heating, and resonance absorption to be described below and the corresponding radiation pressure can produce large-amplitude transient shocks without material preheat. At the low-frequency end of the electromagnetic spectrum, strong broadband emission of coherent far-infrared (FIR) radiation results from the space-charge fields developed in such plasmas. The correlated occurrence of strong x-ray and FIR emission in the laser focus indicates that the dominant radiative processes are driven by a pondermotively induced space-charge gradient and electrostatic wave at the critical surface. Since the laser pulse length is short enough to inertially confine the ions, the resulting current density fluctuation between ionic and electronic components will result in a powerful electromagnetic transient or current pulse whose rectified pulseshape is approximately the derivative of the exciting optical pulse. The space-charge mechanism will also accelerate hot electrons which can subsequently interact with the solid target to produce energetic x-rays via a nonthermal bremsstrahlung process. In this case, electron temperature is dominated by the pondermotive potential of those electrons directed along the laser propagation axis since the high-density plasmas produced by short-pulse excitation tend to rapidly thermalize the quiver energy, producing a quasi-Maxwellian plasma with a temperature characterized by the free electron quiver energy. The contribution to bremsstrahlung emission from energetic electrons at the tail end of the velocity distribution for this case is empirically given $T_{hot} \sim (I\lambda^2)^{1/3-1/2}$. An important observation concerning laser plasma x-ray sources is that the production efficiency of thermal x-ray emission (<15 keV) is dictated by how hot the equilibrated plasma becomes and therefore the size of the laser driver, while nonthermal x-ray generation is dictated by the hot electron temperature produced by a nonlinear laser-plasma interaction and is not directly dependent on plasma heating. Consequently, compact short-pulse lasers with relatively modest pulse energies (~100 mJ) and focal irradiance ($>10^{17}$ W/cm²) properties can achieve efficient hard x-ray conversion >10 KeV ($\sim 10^{-1-2}$) and unprecedented spectral brightness by creating an energetic non-Maxwellian electron distribution in a dense overionized cold plasma background. The production of the equivalent x-ray yield using nanosecond laser pulses would require laser installations in the kilojoule range because of the lower conversion efficiency (10^{-4}) available under the constraints of thermalization. Owing to the presence of steeper electron density gradients in short-pulse laser plasmas, the incident laser energy is more efficiently coupled near critical, and a larger fraction can be absorbed by the solid material to produce hard x-rays. Bremsstrahlung emission will be coherently radiated if the ions are strongly coupled in the dense plasma.

The evolution of temperature and density spatial structure due to the interplay of electron diffusion and collisional absorption will sensitively influence absorption fraction, transport rates, x-ray conversion, and the character of heated particle distribution functions. Researchers have found that the fraction of energy absorbed by plasma and the resulting distribution of electron temperature can depend considerably on the steepness of the density gradient and critical surface coupling. The exact physical picture will depend on whether there is a substantial region of underdense plasma formed in front of the target or whether a step-like density profile occurs at the solid-vacuum boundary. The idealized step case is seldom realized because either the optical pulselength is longer than the thermal expansion time ~ps or because of the presence of prepulse which ablates material prior to the arrival of the main pulse and produce a thin plasma layer in the focal spot. When expansion occurs $\sim O(\lambda)$, the standard Fresnel interface equations are no longer valid and the full Helmholtz electromagnetic equation must be employed to calculate absorption in the density profile

which can be subsequently coupled to a set of self-consistent equations for heat flow and ionization. Lack of hydrodynamic equilibrium can strongly influence hot electron fraction and temperature scaling since the pressure balance imposed by long pulse (ns) conditions is unlikely to be achieved for femtosecond pulses. Such a plasma may also exhibit non-Maxwellian and nonstationary effects (Doppler shift) in the emitted spectrum. The strong relationship of plasma transport parameters on density scalelength illustrate the importance of adequate pulse diagnostics and contrast ratios ($>1:10^{-6}$) for meaningful laser-plasma interaction experiments. The presence of a low-intensity background or pedestal from amplified spontaneous emission (ASE) in a low-contrast chirped pulse amplification laser system means that instead of vacuum-solid density, that a preformed plasma with finite density scalelength, albeit steep, exists in front of the target.

Absorption mechanisms and hot electron production for ultra-intense ($I > 10^{17} \text{W/cm}^2$) laser pulses incident on a solid or sharp overdense plasma slab show pronounced deviations from the well-known results reported for low-intensity and long pulse length (nanosecond) laser-plasma interactions. The ultrafast laser interaction conditions described in this report, particularly in the presence of self-channeling which eliminates prepulse, will result in very different conditions from the traditional adiabatic implosion profiles where collisional effects are significant and IB absorption strongly competes with pondermotive self-focussing over long scalelengths in density and temperature [$c\tau_p \gg \lambda_0$, $L_n \gg \lambda_0$]. In particular, a preformed plasma with finite scalelength and $v_{th} > v_{osc}$ will show a predominance of distributed inverse bremsstrahlung absorption originating from electrons that have gained energy from the laser and subsequently lost it in collisions with ions; i.e., the light wave is damped by the plasma which heats up. Historically, intense infrared CO_2 lasers ($I\lambda^2 \sim 10^{16} \text{W cm}^{-2} \mu\text{m}^2$, $\lambda = 10.6 \mu\text{m}$) with nanosecond pulses were utilized to create large preformed underdense plasmas ($L > 100 \lambda_{opt}$) which exhibited considerable distributed absorption into hot suprathermal electrons by nonlinear inverse bremsstrahlung and various parametric laser-plasma interactions, primarily stimulated Raman scattering and two-plasmon decay. This regime is very different from our present case where the normalized amplitude of the electric field of the laser light causes the onset of relativistic electron quiver motion and hot electrons are produced without preheat by localized non-collisional processes involving the oscillatory component of the laser transverse pondermotive force at or near critical, including resonance absorption and vacuum heating. Although fast electron generation is undesirable in the ICF context because of fuel preheat which prevents target compression to necessary densities for gain, the production of such electrons by intense short-pulse interaction is advantageous for generating hard x-rays in the cold overdense target behind the originating plasma. For extreme intensities at normal incidence, energy is transferred directly to ions through formation of a collisionless shock impulse. The ability to *both* create a dense plasma and interact with it at high density is a fundamental change in the laser-plasma interaction paradigm. Inclusion of kinetic effects, collisionless absorption mechanisms, and multi-dimensional transport will be critical for modelling heat flow penetration into the target. A Fokker-Planck treatment accounting for delocalized heat transport and modifications from classical Spitzer-Harm conductivity and distribution functions will replace the diffusion equation. Electron nonlocal closure relations for fully ionized plasmas that are valid for arbitrary collisionality will need to be developed.

X-ray yield will depend on absorption, heating, ionization, transport, and recombination processes. Experimental work analyzing the scaling of x-ray source emission in the 20-100 keV range following irradiation of solid targets with varying laser fluences is consistent with a bremsstrahlung production mechanism. For laser intensities $> 10^{17} \text{W/cm}^2$, a number of collisionless nonlinear processes play a major role in laser energy absorption, particularly for non-normal (oblique incidence angle) p-polarized ($E \parallel \nabla n$) excitation. Under these conditions,

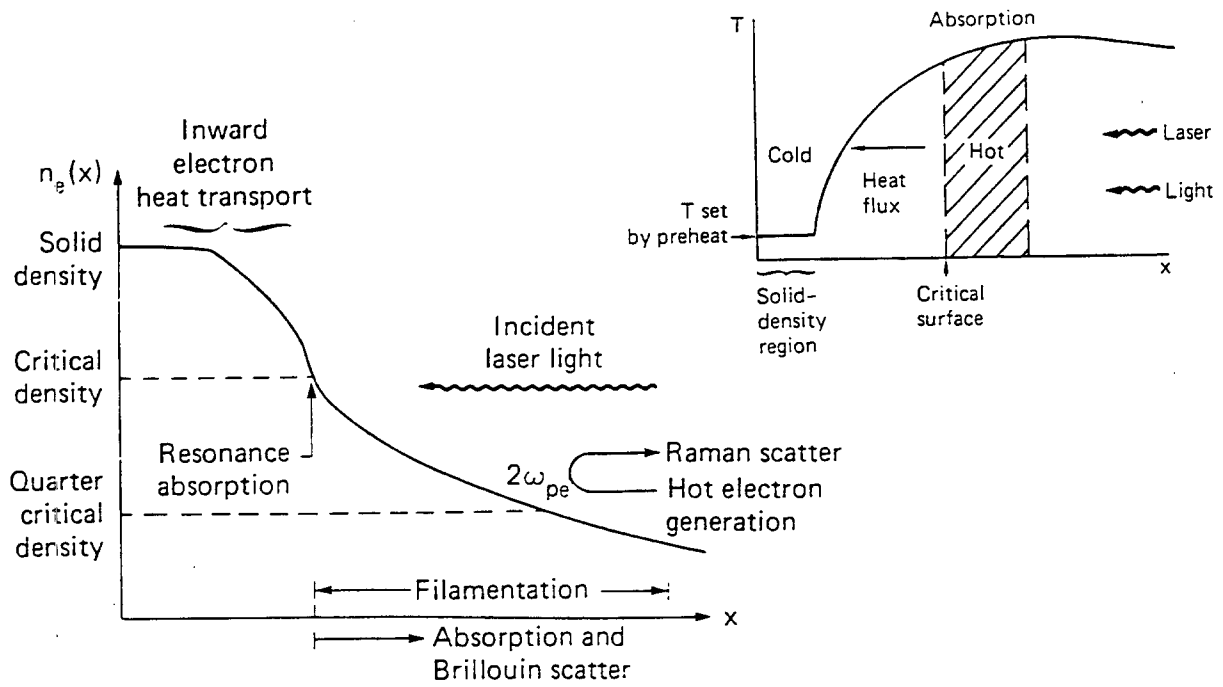


Figure 1: Schematic picture of characteristic electron density and temperature profiles in laser-produced plasma formed from an initially solid target, showing location of major plasma-physics coupling processes and dominant heat transport mechanisms.

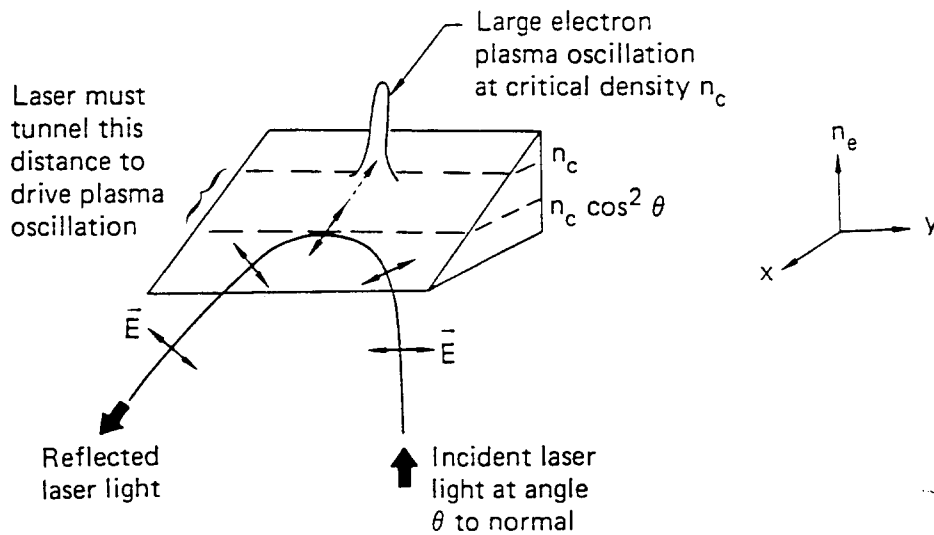


Figure 2: Interaction configuration for resonance absorption of p-polarized light, where E is in the plane of k_L and ∇n_e .

the plasma temperature rises so quickly that collisions become ineffective during the interaction and in addition the electron quiver velocity is comparable to the thermal velocity thus further reducing the effective electron-ion collision frequency ν_{ei} . A complicated mixture of resonance absorption, vacuum heating (Brunel Effect), sheath inverse bremsstrahlung, anomalous skin effect, and relativistic JxB mechanisms driven by the pondermotive force and associated heat flux operating near critical are the alternative to collisional absorption for producing hot electrons in this instance; partitioning of the mechanistic contributions will depend on scalelength and irradiance in a manner not completely understood. When p-polarized light tunnels through the critical surface and resonantly excites a plasma wave (EPW), the resulting wave grows over several laser periods and is eventually damped by collisions at low intensity and by particle trapping and wave breaking at high intensity thereby electrostatically accelerating electrons. These laser-driven fast electrons exhibit a long mean-free-path which can penetrate into the cold region of the stopping target beyond the heat front. They are then converted to nonthermal x-rays in the form of MeV bremsstrahlung continuum via collisions with ions or produce $K\alpha$ fluorescence line radiation by the relaxation of an outer shell electron following K-shell ionization. Particle-in-cell and relativistic Vlasov kinetic simulations for the nonlinear dynamics in the intense laser field predict that for typical conditions the absorption rate can exceed 50% and that most of this energy is transferred into the solid by fast nonthermal electrons (25% of these electrons with energies ~ 1 MeV). Exceeding large self-generated magnetic fields can be created and convectively magnified by these electron interactions and these fields will dramatically impact 2-D lateral transport and pondermotive hole boring. Multi-dimensional effects associated with rippling of the electron critical surface will improve the efficiency of resonance absorption even in the case of steep gradients.

Schnurer measured x-ray production in the energy range of 100 keV from picosecond laser-solid interactions at focussed irradiances approaching $7 \times 10^{17} \text{ W/cm}^2$ and showed an intensity scaling of x-ray yield proportional to $I\lambda^{2.8}$. Kmetec showed that the detected yield increases as $ZE^{3/2}$ at laser intensities $\sim 10^{18} \text{ W/cm}^2$, where E is the laser energy per pulse and Z denotes the target atomic number, and measured .3% conversion efficiencies ($4.5 \mu\text{J/sr}$) from tantalum in the 20-300 keV range using a laser energy of 40 mJ. The results were shown to be physically analogous to an electron-beam driven x-ray tube where the target is the anode and the cathode-anode voltage scales as a function of the laser intensity. Researchers at Lawrence Livermore have reported production of suprathermal electrons (5% @ 25 keV) and efficient secondary $K\alpha$ fluorescence (10^{-5}) in the 8-30 keV energy range for solid Zn, Ge, Mo, Sn targets using a hybrid Ti:S/Nd:glass CPA laser (~ 400 fs, 700 mJ, $\lambda = 1.06 \mu\text{m}$). Similar conversion scaling has been observed by Rhodes, et al in solid BaF_2 (1-2% ~ 1 keV) and in xenon cluster jet (Xe(L) $\sim 4-5$ keV) for ultraviolet short-pulse laser excitation of comparable intensity.

High-order harmonic generation at the vacuum interface and cold $K\alpha$ radiation produced by hot electrons deposited in the overdense solid offer the shortest x-ray emission durations and are limited by the laser pulse and the electron thermalization time, respectively. In addition, both signatures are monochromatic, quasi-monochromaticity being achieved in the $K\alpha$ case because the temperature increase due to electron energy deposition (which would produce a weak wavelength shift) is small. The resulting monochromatic signatures will be useful for differential absorption imaging and in combination with fast temporal gating will facilitate high spectral brightness offsetting the reduced conversion efficiencies. $K\alpha$ photon emission is inherently a sensitive diagnostic for detection of hot electrons produced near the critical surface. Broad bremsstrahlung continuum emission will have utility for opacity and edge-shift measurements, and the flat unstructured background as function of photon energy will allow

systematic optimization of contrast for shadowgraphic imagery in backlighting/radiography applications.

Eventually all the energy absorbed by electrons is transferred to ions (some may be radiated) as the target disassembles. This occurs in a hydrodynamic timescale well after the pulse has interacted with solid/plasma. At ultrahigh intensities, ion motion can alter the electron dynamics by changing the density profile (profile steepening) near the critical surface and by creating conditions for induced transparency. A strong space-charge generated by electron circulation in the vicinity of the surface can push out an underdense shelf which can drastically change absorption behavior. Light pressure (pondermotive force) from the laser can also compete with the thermal expansion force in short-scalelength plasmas to directly accelerate ions inward with a velocity measurable as a red Doppler shift in the unabsorbed light reflected from critical. Pondermotive hole-boring several wavelengths deep in overdense plasma can result from a combination of three requisite effects (1) light pressure which exceeds the thermal plasma pressure and pushes plasma inward, (2) radial pondermotive force ∇I which pushes electrons from the center of the laser beam creating a charge separation which pushes ions exterior to the interaction zone, and (3) enhanced skin depth where the laser spatial intensity profile is greater due to the relativistic increase in effective plasma frequency:

$$\omega'_p = \omega_p / \gamma; \quad \gamma = [1 - (v_{osc}/2c)^2]^{1/2} \quad [1]$$

inducing transparency when the laser beam is transmitted through nominally overdense plasma without reflection. As the hole is formed, absorption and hot electron temperature both increase because strong density gradients are formed parallel to the laser electric field. These gradients will also generate a magnetic field by a $d\mathbf{B}/dt \sim \nabla n \times \nabla T$ mechanism. If the leading edge of the laser pulse is sufficiently sharp with respect to the ion response time, a collisionless ion shock can be produced with an electron temperature in back of the shock >100 keV and further enhance skin effects at the plasma interface.

• *Relativistic Self-Channeling*

Short-pulse laser propagation in fully ionized underdense plasma is affected by a variety of phenomena including relativistic self-focusing, plasma wave generation, and pondermotive channeling. In general, self-focussing or refractive guiding occurs when the plasma index of refraction $n = [1 - (\omega_p/\omega_0)^2]^{1/2}$ exhibits an intensity-driven spatial variation arising from the nonlinear response of the dielectric. Superposition of two counterbalanced nonlinear contributions to the effective refractive index profile can create a steady-state channel or waveguide structure if the rate of self-focussing matches the diffractive divergence and plasma defocussing due to photoionization. The relativistic mass increase of electrons due to quiver motion in the laser electric field ($a_0 > 1$) and the corresponding electron density decrease (charge displacement) of radial pondermotive expulsion are two such superimposed mechanisms to the refractive index which can create a suitable variation for stable confinement of propagating radiation over a range of physical conditions if the critical power threshold is exceeded. During the dynamic process, the ions are stationary and the electron density reacts instantaneously to establish force balance between the pondermotive and electrostatic components. Electrons are pushed out of the focal volume by the enhanced pondermotive force $\nabla^2 E$ resulting from the relativistic self-focussing action; changes in the refractive index depend on modifications to both the electron mass (and plasma frequency) and the channel electron density. Additionally, relativistic electrons traveling with the light pulse may generate magnetic fields that pinch the radial electron distribution in stable

magnetohydrodynamic modes. Pondermotive force associated with the self-focused laser can create cavitation (expel electrons) and electron density minima on-axis to produce a radially-dependent focussing index guide while tunneling and multi-photon ionization in the focal region has the opposite laser defocussing effect by producing higher electron densities. The basic envelope equation for the nonlinear current J can be written:

$$(\partial^2/\partial t^2 - c^2 \nabla^2)A = J_{NL} = N_e A / \gamma \quad [2]$$

Here, the source term contains both coupling of the laser field to the plasma and self-focussing. The compensatory balance between refraction in the ionized plasma column and intensity-dependent self-focussing will produce a robust multi-foci structure as shown in figure 3.

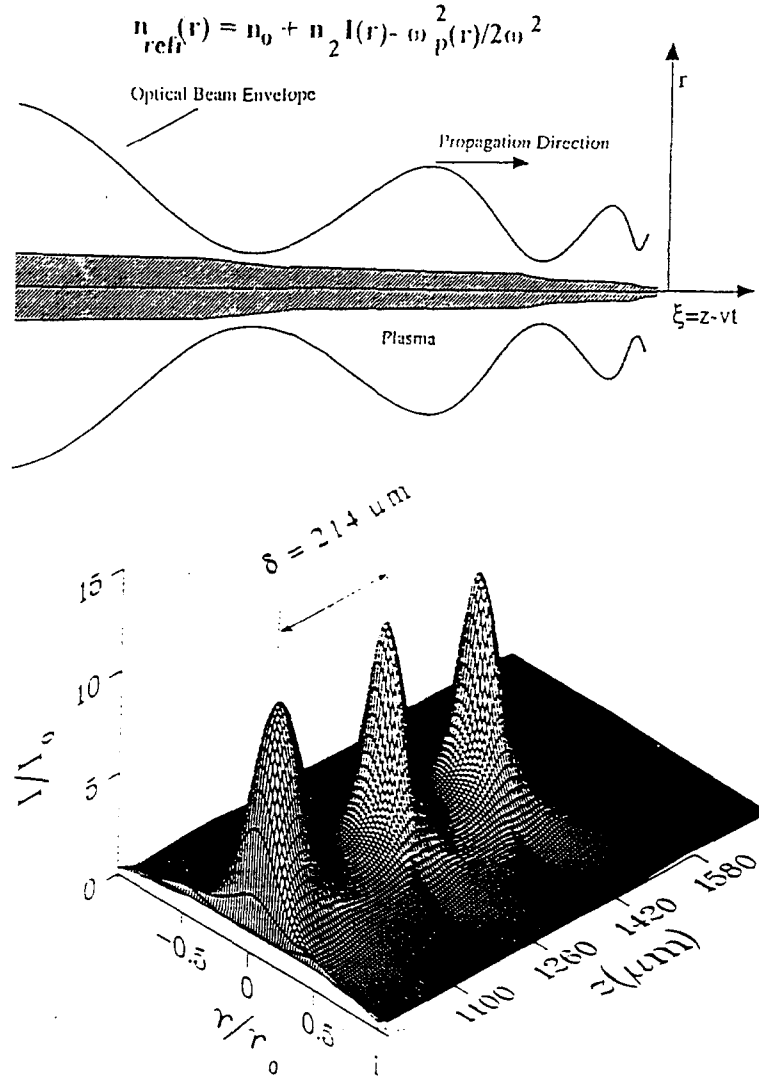


Figure 3: Repeated multi-foci refractive guiding structure predicted by the balanced interplay of relativistic self-focussing and charge displacement nonlinearities. Insert NLSE simulation shows the longitudinal profile of the resulting channel for typical laboratory conditions.

For laser pulses with peak powers above the theoretical relativistic filamentation threshold $P_{cr} > 17(\omega_0/\omega_{pe})^2$ GW, three-dimensional PIC codes predict the formation of a longitudinally-extended narrow propagation channel in high-density plasma with a trapped power of order $10^{3-4}P_{cr}$. The governing (3+1) nonlinear Schrodinger equation (NLSE) defines a self-guiding solution for the complex field which results from the interplay between natural diffraction and intensity-driven nonlinear focussing and ionization-induced refractive defocussing contributions in the plasma dielectric response and which is stable over many Rayleigh lengths. Superposition of these mechanisms on the intrinsic index profile acts to define the propagating energy in a dynamic self-guiding longitudinal waveguide structure which is stable for power transmission and compression. The resulting laser-driven channel is hypothesized to support a degree of soliton-like conductance behavior, simultaneously stable in the space and time domains (group velocity dispersion balances self phase modulation).

The rigorous theoretical formulation combines Maxwell equations with corresponding expressions for the relativistic hydrodynamics of the electron density of a cold collisionless underdense plasma. Four phenomena are explicitly included in this formulation of the NLSE: (1) nonlinearity of the dielectric response owing to relativistic mass shift, (2) variation of the dielectric response resulting from the motion of electrons driven by the transverse pondermotive force, (3) diffractive defocussing, and (4) refraction from radiation generated by (1) and (2), and the initial inhomogeneity of the electron distribution in the plasma column. The governing envelope equation transformed to the moving coordinate frame can be written:

$$\partial a / \partial z + (i/2v_g)[\nabla_{\perp}^2 + N_{e0} - Ne/\gamma]a = 0 \quad [3]$$

$$N_e = N_{e0} + \nabla^2 \gamma$$

where a_0 is the vector potential in the Coulomb gauge, ∇_{\perp}^2 is the transverse Laplacian, and N_{e0} is the initial electron density. In this formalism, the inclusion of group velocity dispersion (GVD) and other longitudinal dispersion effects leading to modulational instabilities or pulse erosion will require higher-order terms be retained in the wave operator. Representative plots of normalized radial ($z_1 \rightarrow z_4$) and axial intensity $I(r, z)$ distributions with the corresponding electron density in an evolving self-focussing channel influenced by the relativistic mass shift and the displacement of the electronic component of the plasma are shown below. Related basic physical mechanisms operating in the highly nonlinear interaction, including plasma wave generation in the form of self-modulated wakefields, are also delineated for completeness of description.

The dynamics of laser channeling will also naturally promote the development of an abrupt time-front to the propagating pulse, since the focussing action is strongly nonlinear and requires a critical power to become effective. All weak light at the trailing edges of the incident optical pulse such as ASE or prepulse which are below the critical power threshold for self-focussing will diffract away rapidly to insignificant levels and not undergo channeling. When the laser pulse duration is comparable or longer than the plasma period ($\tau > 2\pi/\omega_{pe}$) ~ 300 fs and $P > P_{cr} \sim 10^{18}$ W/cm², a self-modulated laser wakefield acceleration (SMLWA) process can generate relativistic electrons and guide injected electrons by resonant coupling of the transverse laser field to longitudinal electron plasma waves ($\lambda_p \sim 100$ μ m). Laser wakefield acceleration and channeling can be synergistically integrated as an optimization strategy for a new generation of x-ray sources utilizing high-intensity ultrafast lasers. By uniting these two processes, it will be possible to simultaneously control power density on target and fast electron production. Based on the number of electrons produced in recent

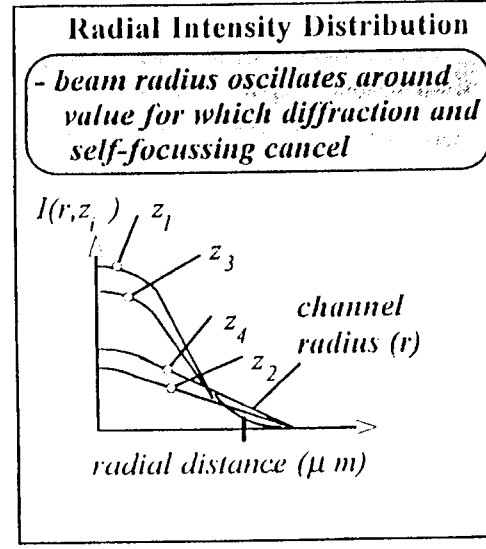
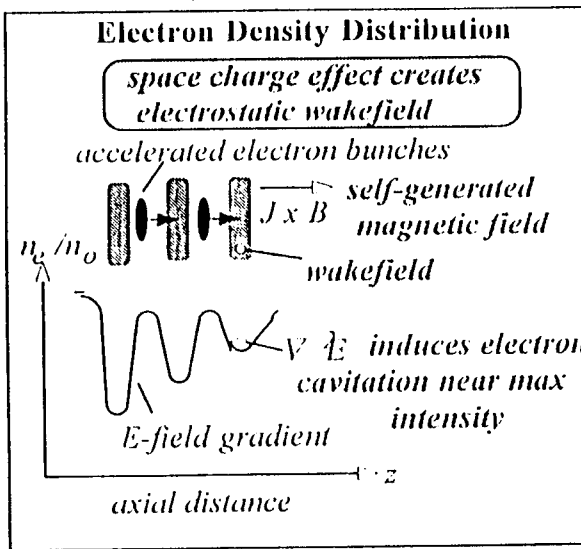
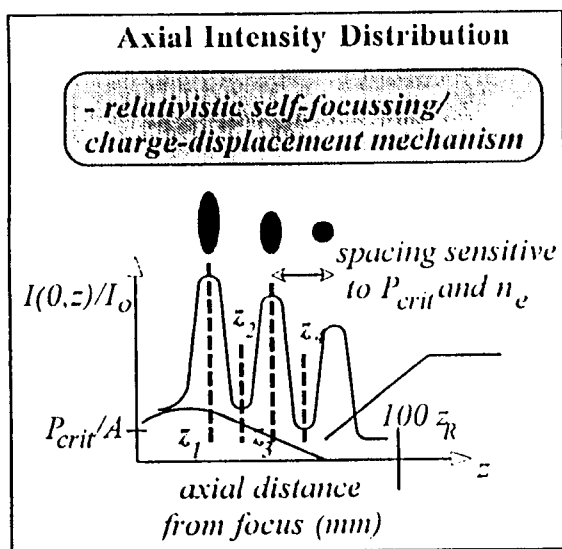
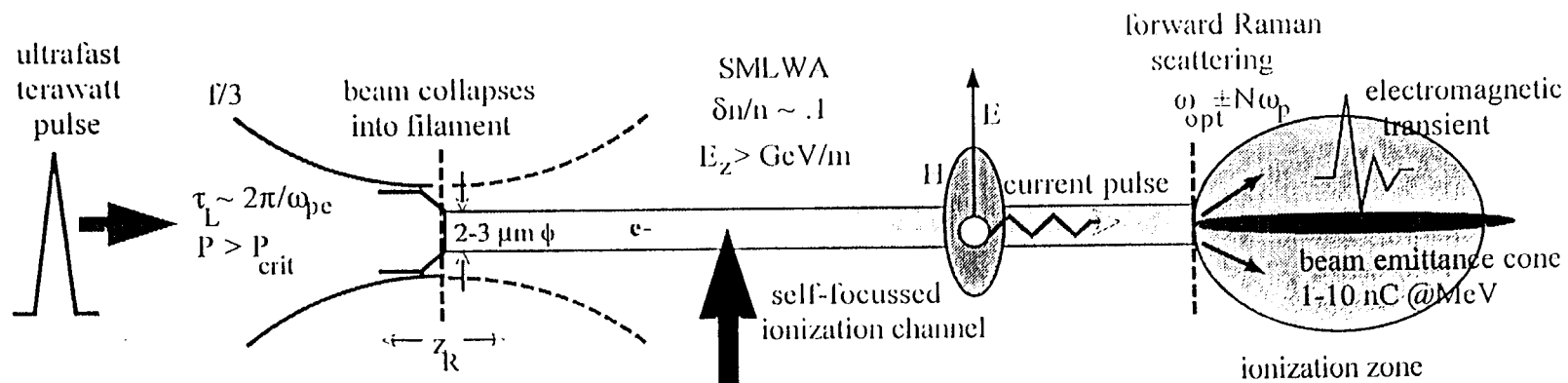
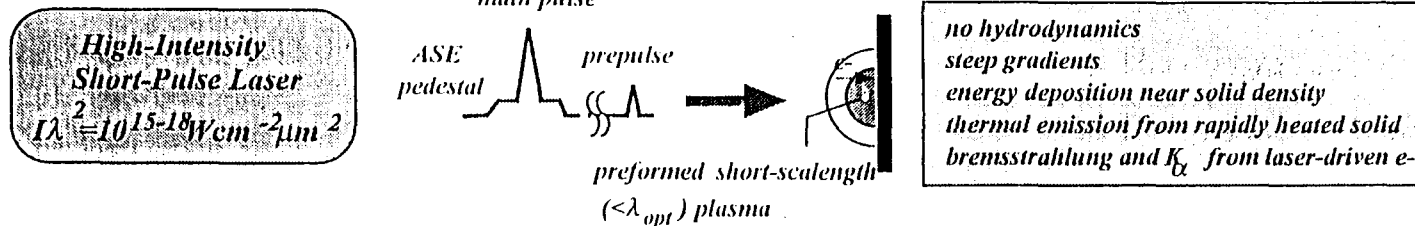
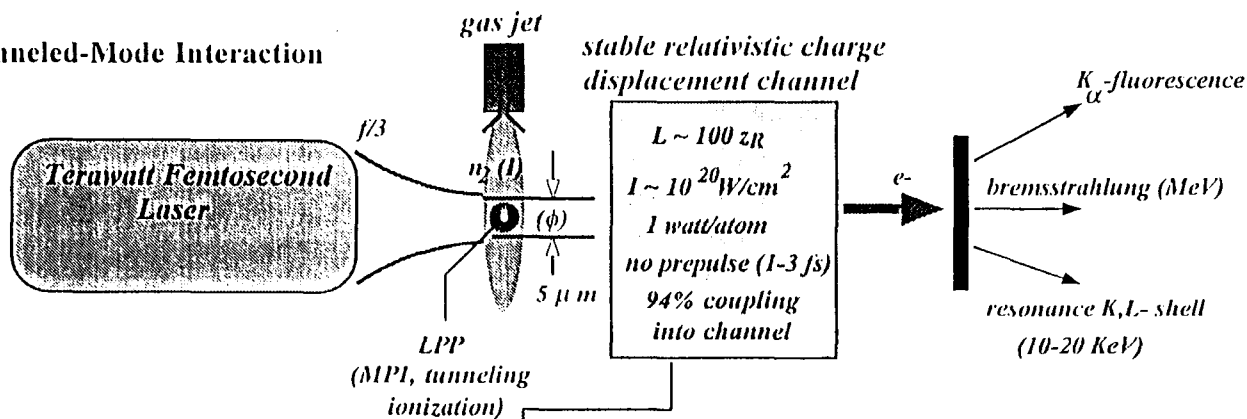


Figure 4: Morphology of the laser-driven channeling process showing beam collapse and subsequent generation of a current pulse and wakefield. Power compression at high-intensities without diffractive divergence will significantly benefit applications to recombination x-ray lasers, fast ignitor schemes, and particle acceleration which require extended interaction regions over several Rayleigh lengths.

(A) Short-Pulse Nonlinear Interaction



(B) Channeled-Mode Interaction



(C) Accelerated Electron Interaction

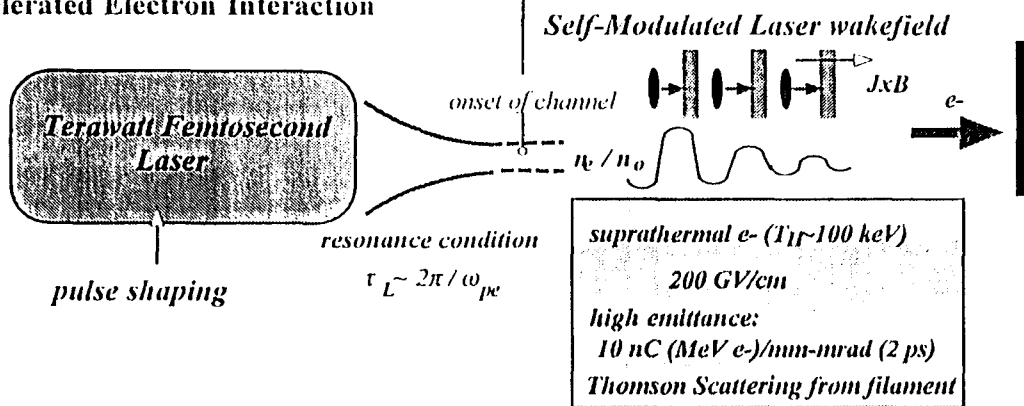


Figure 5: Experimental progression to a new generation of high-brightness x-ray sources which are capable of generating hard x-rays >20 keV. Short-pulse nonlinear interaction with solid targets is augmented by the use of channeled-mode propagation and accelerated electron beams in the laser field.

reported laser wakefield experiments (10^{10} e- with energies .5 -2 MeV, 1.5 ps FWHM) , and assuming a conservative one-to-one conversion of MeV electrons to x-ray photons in the 100 keV range, we can potentially enhance source brightness by an order of magnitude over unassisted methods.

• *Anomalous Coupling Physics*

An analysis of the channeling process involving a relativistic self-focussing charge displacement mechanism indicates that the propagating electromagnetic pulse can produce unique excitation conditions which can not be accounted for by a conventional coupling interaction based on independent single-electron processes. Instead, excited states produced in this manner by the intense external field exhibit an augmented coupling ($> \times 100$) relative to electron collisional studies obtained from EBIT through induction of spatially-ordered coherent multi-electron motions within the channel interior. This test can be performed by a straight forward matching of the radiating ionic states produced by the multi-photon cluster interaction with equivalent charge-state spectra arising from EBIT excitation. Since the EBIT process only involves the scattering of individual electrons from isolated atomic systems, the ions produced are unambiguously generated by conventional single electron-ion interaction electrons. This definitive comparison was made for data obtained from studies of multi-photon induced Xe(L) emission from clusters as described below. These new physical processes enable the dynamic production of so-called "hollow atoms" with inverted electronic configurations in which outer electrons of the atomic system are simultaneously and selectively arranged so that the overall configuration formed exhibits the maximum radiative rate possible at the emitted wavelength; i.e., dynamical orbital collapse drives super x-ray emission.

Recent experimental evidence has shown that high-intensity short-pulse ultraviolet multi-photon production of inner-shell x-rays from rare gas atomic clusters can be combined with the relativistic channeling mechanism to create the prerequisite local atomic conditions and extended spatial organization for realizing efficient x-ray amplification ~ 5 keV Xe(L). The resulting spectroscopy provides direct evidence of an enhanced mode of electromagnetic coupling correlated with self-focussing/charge displacement channeled propagation mechanism in which highly ionized xenon atoms possess a large number of inner-shell vacancies while retaining several electrons in relatively weakly bound outer orbitals. In this process, laser-driven photoelectrons ejected along the ionization channel produce copious core-excited ions with deep vacancies (Auger) that promptly emit energetic x-rays. Delivery of high local power density over a spatially confined region can produce the necessary conditions for inner shell ionization and the resulting hollow atom configurations exhibit improved scaling relationships between excitation power and x-ray gain. In the atoms that constitute the cluster, the intense laser field induces a forced coherent oscillation of the weakly bound outer electrons or an oscillating charge cloud (quasi-particle) which undergoes efficient energy transfer to the inner shell provided certain relationships between irradiance intensity and cluster size are maintained. Coherent multi-electron motion induced by the external drive field simulates the behavior of a particle carrying high charge thereby transforming the fundamental coupling strength for interaction of electrons with matter from the customary value of the fine structure constant $\alpha=1/137$ to an enhanced value approaching $N^2\alpha$ where N is the number of electrons participating in the oscillation. For high-Z targets such as uranium ($Z=92$), the coupling strength enhancement can approach a factor of 10^3 . The strong coupling means that processes involving multi-electron ejection from an inner shell can occur with high probability and scale with atomic number favoring heavy atoms. For the short-lived ordered electron ensemble to be produced, the externally coupled optical field must be large compared to an atomic unit and because the light waves

present a time-varying oscillation for the electrons, the acceleration impressed on the excited electrons must be established in a “turn-on” time in the range of femtoseconds consistent with dephasing limitations for electron-electron interactions. This suggests that radiation of long wavelength or period cannot be effective in energizing the ensemble in a sufficiently compact form for enhanced coupling and corresponding strong x-ray generation. Conversely, short-wavelength radiation, can be effective in driving the multi-electron coupling and consequently exhibit strengthened x-ray generation. The dependence of the strength of interaction, as indicated by x-ray emission characteristics, on the wavelength of excitation provides a simple test of the envisaged enhanced cooperative many-electron coupling mechanism. Recent experiments comparing the x-ray spectrum from xenon clusters irradiated with short-pulse lasers operating in the ultraviolet (248 nm) and near-infrared (800 nm Ti:S fundamental) regions, show the two classes of predicted limiting behavior. One observes very significant differences in the spectrally-integrated strengths (total x-ray emission) with a marked decrease in the peak intensity for the infrared wavelength. With regard to the comparison of the spectral structure, the 800 nm-induced signal exhibits only relatively low Xe^{q+} charge states (27,28,29) and no double-vacancy $(2p)^2$ emission is detected; double vacancy states are highly unusual excited states in which two inner shell electrons are simultaneously absent. These comparative experimental findings lead to the conclusion that the use of sufficiently intense femtosecond pulses of sufficiently short wavelength radiation enables one to modify the coupling and deposition of radiation in matter. This new regime of strengthened physical interaction could serve many important applications including micromachining, generation of high-brightness x-ray sources, and new unconventional forms of nuclear energy production.

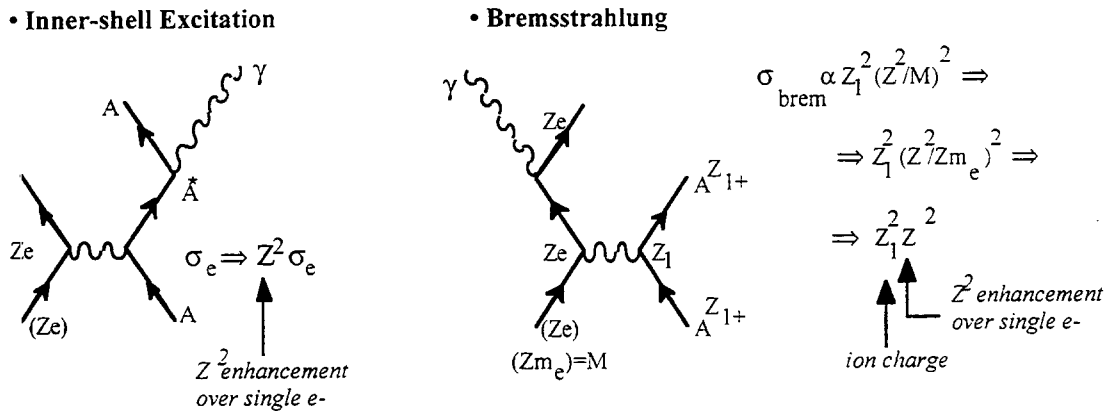


Figure 6: Hypothetical Feynman representation of enhanced coupling physics resulting from ordered coherent multi-electron motion in the spatially-localized laser-driven channel.

III. Experimental Accomplishments

• *Laser System*

The laser system employed in the present experimental study is illustrated schematically in figure 8. A sub-picosecond (~250 fs) KrF excimer/Ti:sapphire hybrid laser operating in the ultraviolet ~248 nm was focussed by an f/3 off-axis parabolic mirror into a differentially-pumped jet gas cell. The focussable intensity approached a maximum of $10^{19} W/cm^2$ and the

Z - λ Imaging of Xe X-Rays

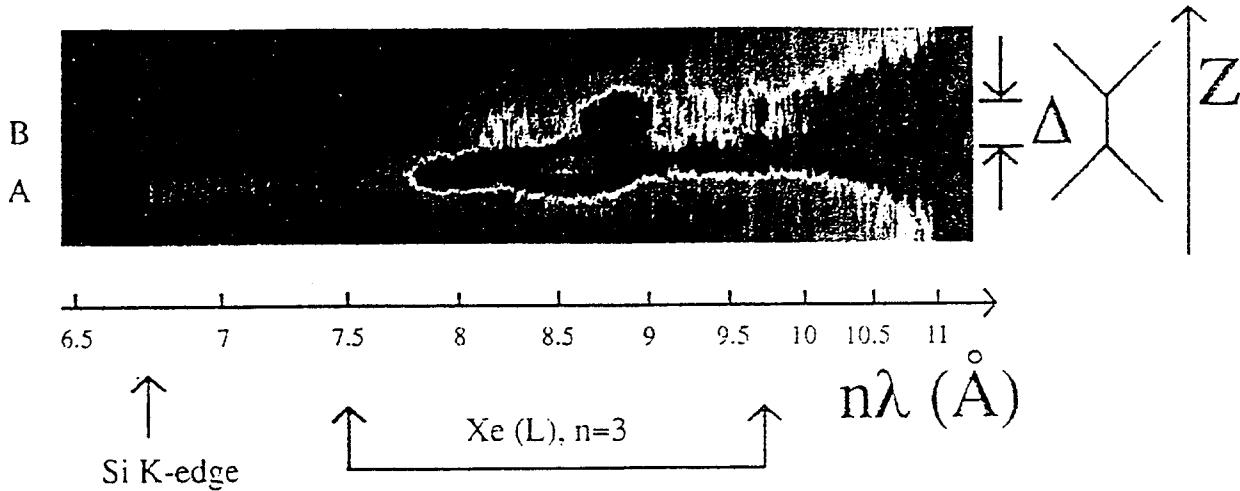
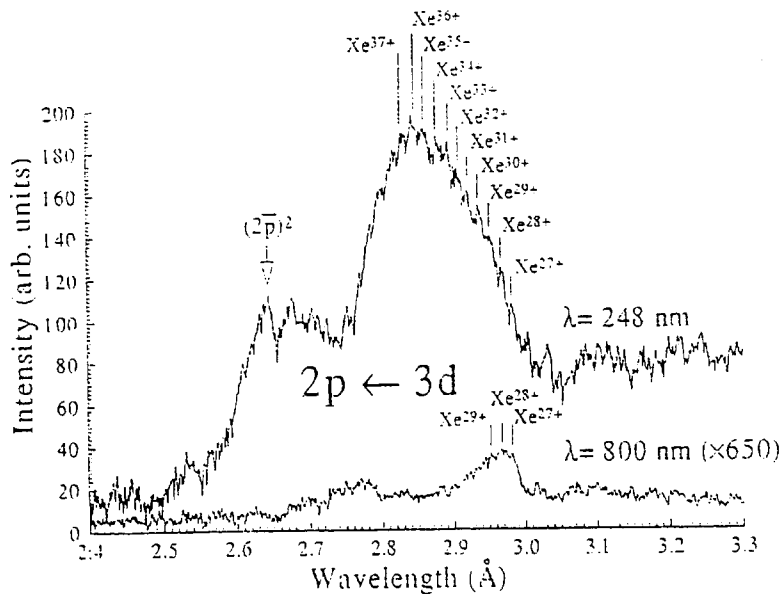


Figure 7: Spatially-resolved ($Z-\lambda$ imaging) Xe(L) emission spectrum showing enhanced x-ray production in the channel region denoted by (Δ) on the ordinate; abscissa designates the wavelength. The color scale is defined by black (zero), red through violet ascending intensity and white (maximum). Corresponding spectral line-out shows pronounced enhancement of the coupling strength and evidence of anomalous $(2p)^2$ transition.



peak power ($\sim .7$ TW) exceeded the critical power for relativistic self-focussing. The laser architecture employed a conventional titanium sapphire chirped pulse amplification front-end (oscillator and regenerative amplifier) which was frequency-tripled and subsequently amplified in a 4-pass KrF laser module. The target was hydrodynamically produced by a cooled high-pressure pulse valve fitted with a circular sonic nozzle.

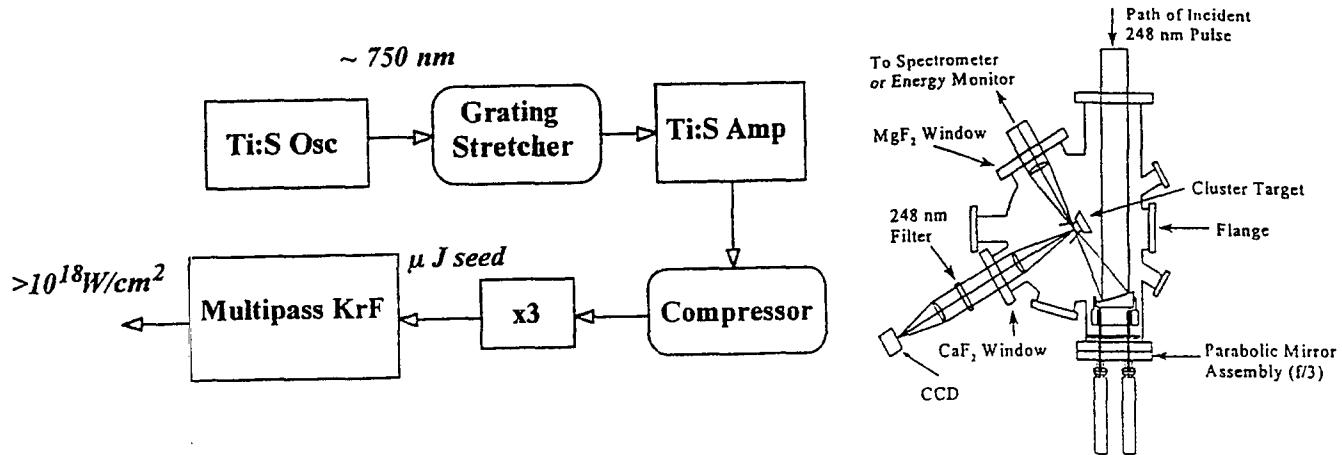


Figure 8: High-brightness ultraviolet sub-picosecond terawatt laser (nominally ~ 250 fs, 300-500 mJ, $> 10^{21}$ Wcm $^{-2}$ sr $^{-1}$) using frequency-converted Ti:S seed. Also shown is the chamber geometry for the laser-plasma interaction experiments.

• *X-ray Spectra*

In collaboration with Professor Charles Rhodes' research group at the University of Illinois-Chicago, we used a self-focused femtosecond ultraviolet terawatt-class laser with a focal irradiance exceeding 10^{18} W/cm 2 to produce L-shell x-ray emission from gold-coated solid targets. Short-wavelength spectra >10 keV were acquired using an imaging von Hamos crystal spectrometer operating in 7th-order mica with an aluminized polycarbonate/kapton/titanium filter set. The single-shot integrated x-ray yield (estimated) near 10-14 keV exceeded our predicted value of 1 mJ per 2π steradians and the observed spectrum although occurring generally in the expected spectral region for Ne-like Au transitions with charge state range (55+), exhibited a predominant asymmetrical (blue-shifted) broadband feature (~ 700 eV) superimposed on bremsstrahlung continuum and sharp spectral line emission ($L\alpha\beta\gamma$). The appearance of the data is quite similar qualitatively to the case for Xe(L) emission previously observed from high-intensity short-pulse irradiation of xenon clusters and very different from Ne-like atomic spectra reported in the literature for conventional excitation mechanisms. Specifically, the customary L-shell spectrum at low average plasma density (EBIT case) is dominated by a few sharp lines; in contrast, it is evident that the multiphoton-produced spectrum is dominantly a single broad feature. The feature is attributable to nonthermal core-excited d-p transitions in an atom that possesses a large number of $n>3$ electrons. Because of the presence of outer-shell electron interactions, the allowed transitions become distributed over a wide spectral band. This characteristic is direct evidence of a dynamical "hollow-atom" excitation mechanism in which the energetic laser field collectively drives correlated multi-electron motion to produce anomalously strong coupling in the propagation channel. To our knowledge, this is the first reported measurement of gold L-shell

emission from a laser-produced plasma and is the direct result of the unique interaction conditions which can be obtained with high-intensity short pulse lasers. The radiating source size was measured from the von Hamos focal width to be < 10 microns.

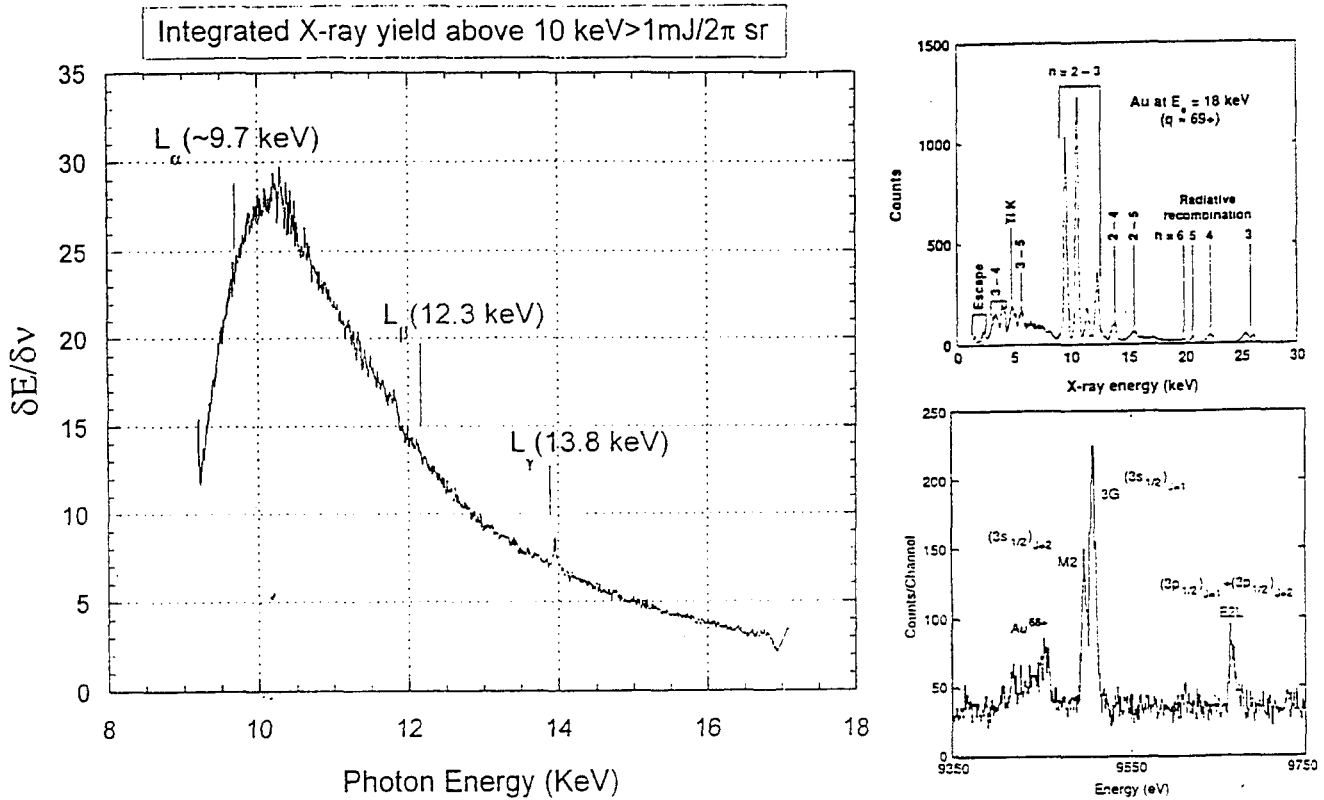


Figure 9: X-ray emission (L-shell) from gold target excited by short-pulse high-intensity ultraviolet laser. The laser conditions for the experiment were 240 mJ pulse energy, 250 fs pulse duration, $f/3$ focussing optic. The imaging crystal spectrometer was of von Hamos type (7th order mica) with an aluminized polycarbonate/kapton/titanium filter set. Preliminary spectral assignments are noted but will require further analysis. Note difference with EBIT spectrum shown for comparison.

We are pursuing ongoing experiments for uranium L-shell (15-17 KeV) emission and other $K\alpha$ and K-shell candidates in the 10-50 keV energy range. Most recently, results from tantalum foils ~ 25 -100 μm thick show new highly favorable properties for hard x-ray generation versus solid target geometries with estimated conversion efficiencies >5%. Preliminary spectral evidence shows transmission of a significant component of the resulting x-rays through 100 μm of Fe and 50 μm of Au, indicative of a large source yield above 20 keV. In these experiments, we also observed reproducible hole-drilling through 75 μm of Ta in a single shot with ~ 300 mJ of pulse energy. The resulting bore hole was radially symmetric with a 50-70 μm (aspect ratio of exit and entrance apertures was 1:1) diameter and exhibited no evidence of melt, refractive turning, or explosive shock. We conjecture that power compression in the self-channeling process can create the requisite conditions for electron bunching (SMLWA) and magnetically-confined pinching (sausage mode) mechanisms which dramatically increase power deposition (> 10 W/atom) and energy coupling in the solid material to achieve near-complete vaporization. The interaction physics may be related to recent photoionization and fragmentation phenomenology observed in laser-driven cluster microplasmas observed at Imperial College. Clusters are small tightly packed groups of atoms.

in this case estimated to be on average 20-30 atoms/cluster. These systems are useful to regard as large molecules whose local atom density resembles solid matter.

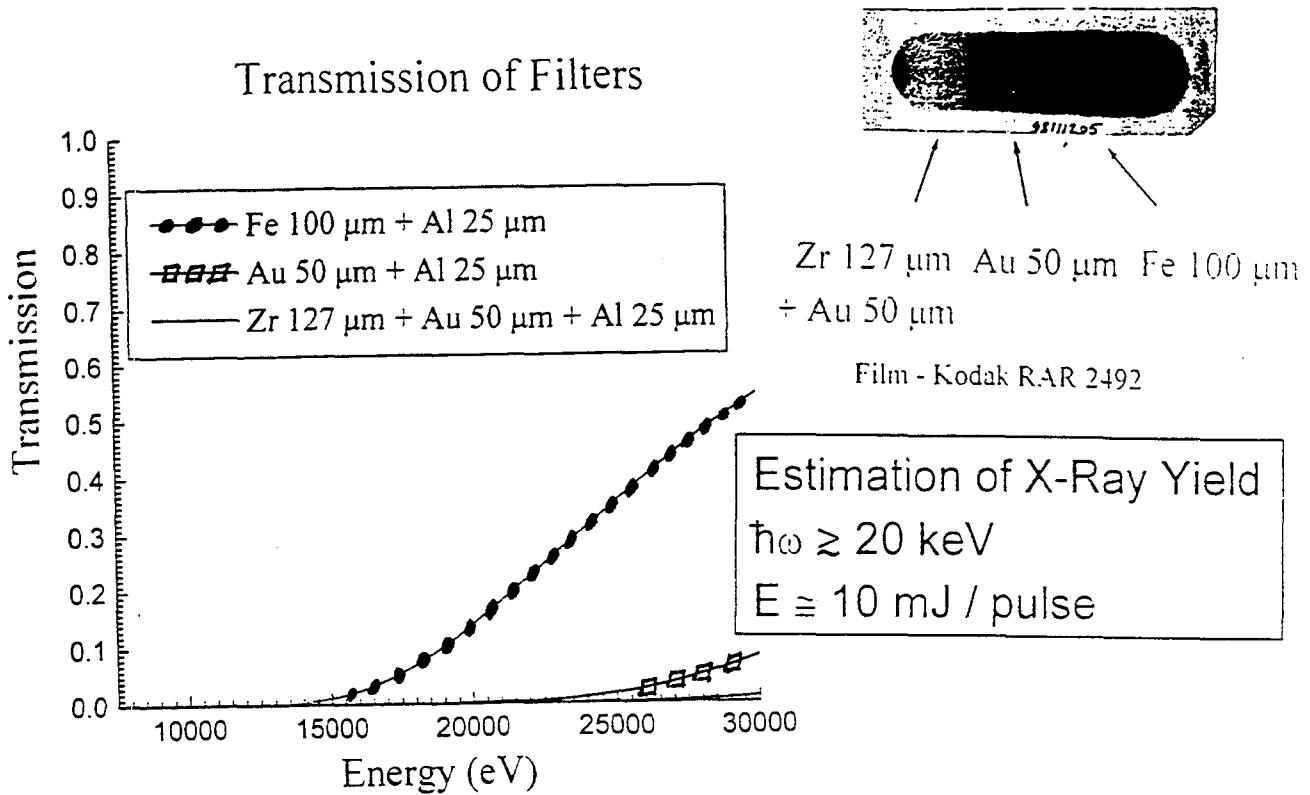


Figure 10: X-ray yield measurements for Ta thin foil showing the filter transmission curves as a function of energy. Note that the film sensitivity (Kodak RAR 2492) is decreasingly sharply at the higher x-ray energies. The corresponding laser parameters are: $\lambda = 248 \text{ nm}$; $\sim 350 \text{ mJ}$; $\sim 270 \text{ fs}$; $f/3$ focussing. Estimated yield above 20 keV is 10 mJ per pulse!

• *Diagnosis of Relativistic Channeling*

Corroborative measurements of the self-trapping channeling morphology with spatially-resolved Thomson scattering and x-ray pinhole imagery indicated the presence of a stable longitudinally-extended filament structure exceeding 50 Rayleigh lengths with a $< 5 \mu\text{m}$ radial extent. Direct visualization of the spatial distribution in xenon cluster targets using electron density and x-ray signatures confirmed the existence of a zone of confined propagation exhibiting longitudinal and radial extent in excellent agreement with theoretical predictions for the relativistic self-focussing charge displacement mechanism. In performing these diagnostics, single-shot Thomson signals scattered transversely to the laser direction were imaged on a CCD camera for a variety of irradiation and pulse-valve conditions using a relay magnification system. The spatial resolution of the optical system was verified with a calibrated test pattern to be $5 \mu\text{m}$ and a narrow band filter was used to admit the scattering signal at 248 nm while rejecting interfering component produced by the plasma. It is important to note that the pattern of scattered radiation is a chord-averaged quantity which will depend on the intensity and density profile along the observation axis (eg. the line integral). In the data, the appearance of a thin dark central region is consistent with

reduction of the electron density in the central core of the high-intensity zone of the propagating channel- the expected signature of radially-driven pondermotive electron cavitation. The collapse diameter is currently limited by the spatial resolution of the imaging system (theoretical prediction 1-2 μm) and the power density in the channel was estimated as 10^{19} W/cm^3 . X-ray emission from the channel region is expected to be a highly specific signature of the energetic conditions produced in the self-focussing interaction, and filtered pinhole images showed strong evidence of filamentary structure co-registered with the Thomson data. Strong electromagnetic transients and coherent far-infrared emission at THz frequencies were also detected as the result of space-charge fields generated at the focus of the optical pulse due to the large pondermotive force. Preliminary indirect evidence of hot electron filaments or streamers generated by a wakefield or current pulse mechanism exiting the channeling process and causing impact ionization were observed. Future experiments will look for direct evidence of self-modulated wakefields or e-beams by accumulating electrons in the forward direction using an electron spectrometer or by measuring self-generated second-harmonic generation and modulational instabilities (ASD, Raman) in the laser spectrum. Schlieren interferometry and polarimetric Faraday rotation techniques can be used to probe associated density perturbations and magnetic fields.

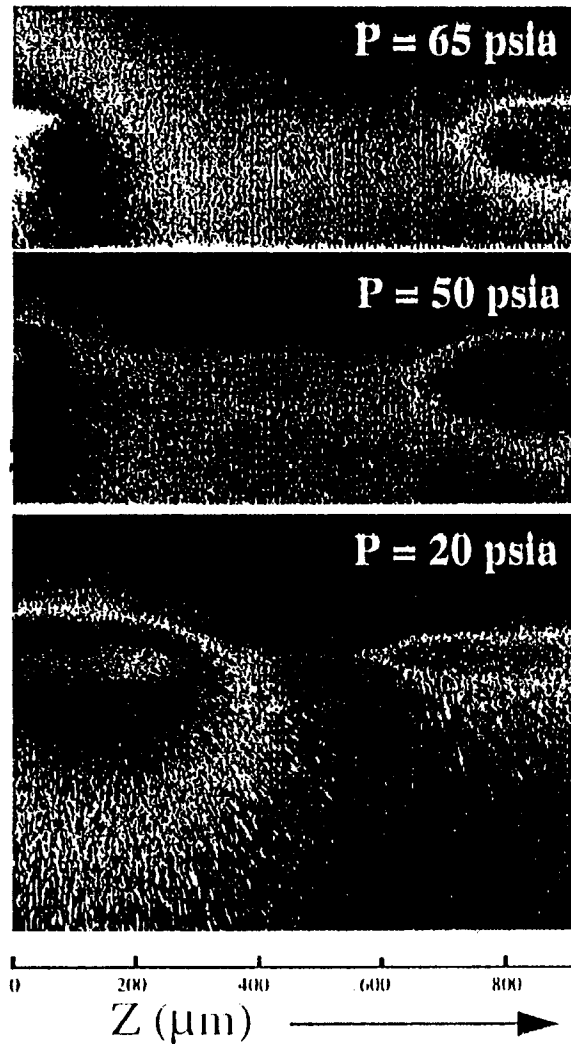
• *X-ray calibration*

As part of the experimental campaign, we also used the short-pulse x-ray bursts (recombination time < 5 ps) created by M-shell xenon (~ 1 KeV) and L-shell barium fluoride ($\sim 4-5$ KeV) to directly measure the impulse response of vacuum x-ray diode (XRD) and diamond photoconducting detector (PCD) devices whose electrical output is linearly dependent on incident x-ray flux. This information is critical to developing a secondary calibration standard for x-ray diagnostics, particularly in the energy range above 10 keV where a paucity of instrumentation currently exists. For these measurements, heliax cabling was used with a bandwidth > 5 Ghz. The PCD assembly was biased at -100 volts and connected in single-ended mode to the transient digitizer to reduce electrical noise. The measured risetime for both devices, deconvolved for instrument response and Fourier filtered, was found to be approximately 100 ps which may have important programmatic implications for analysis of mix and Rayleigh-Taylor contributions in on-going hydrodynamic evolution studies on Z. Evidence of a strong electromagnetic pulse was also detected using a simple induction dipole antennae loop and verifying absence of a photon path.

• *Modelling Efforts*

In parallel with experiments, modeling efforts have been ongoing toward spectroscopic analysis and developing predictive capability and stability criteria for the channeling mechanism. The theoretical analysis seeks to define stable eigenmodes in the nonlinear Schrodinger equation governing the guiding process and electrostatic force balance in the channel. By correlating the model results with our experimental data such as x-ray spectra and spatially resolved images, we have established first-order optimization parameters and stability maps for efficient x-ray conversion. The basic computational procedure developed in this work will find general usefulness in a variety of cases involving propagation in saturable nonlinear media different than plasma, including Kerr self-focussing in atmosphere.

The existence of dynamic stability is essential for the control of high-power density plasmas. Of particular importance are the physical limitations of stable whole-beam self-channeling behavior, principally robustness to spatial perturbations of the incident laser intensity and the onset of filamentation instabilities, and corresponding implications for maximum achievable power density as a function physical conditions in the plasma. Stable asymptotic forms of the

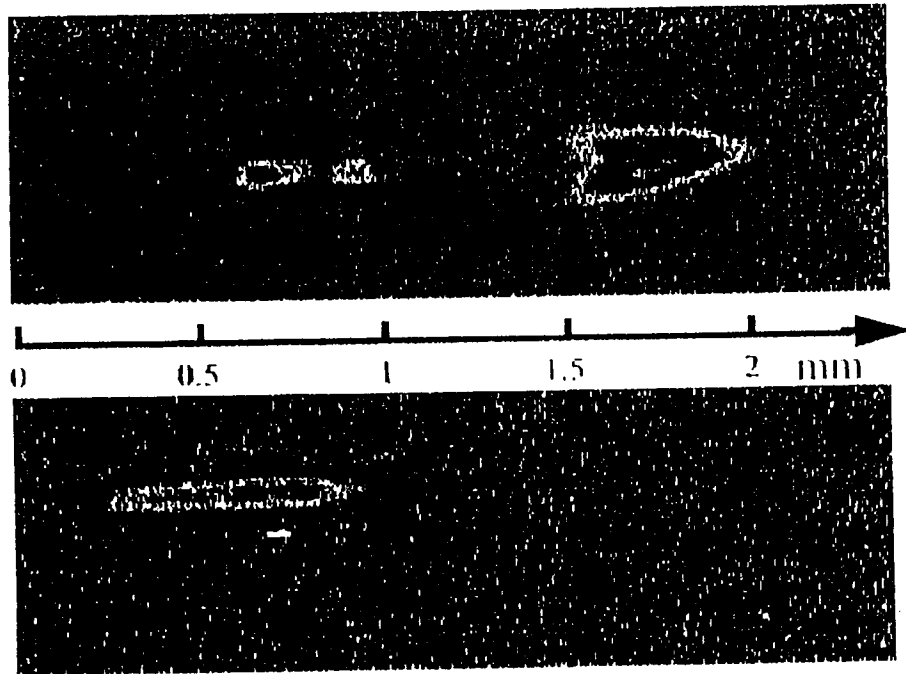


UIC Laser Conditions:
 248 nm , 270 fs, $\sim 250 \text{ mJ}$, $f/3$ mirror

Target Geometry:
 Pulsed Valve with Single Wall

Target Gas:
 Xe, $P = 50 \text{ psia}$, $T = 20^\circ\text{C}$
 Nozzle diameter = 1.5 mm
 Rayleigh Range = 28.5 mm

Figure 11: Transverse image of Thomson-scattered light at 248 nm from a self-channeled laser filament as a function of pressure in the xenon cluster gas jet. The direction of laser propagation is noted. Rayleigh range of $f/3$ focussing system was 28.5 μm .



$P= 35 \text{ psia}, T= +10^{\circ}\text{C}$

$P= 140 \text{ psia}, T= -35^{\circ}\text{C}$

Rayleigh Range $\sim 28.5 \mu\text{m}$
 Target Gas: Xe
 Target Geometry:
 Pulsed Valve with a Wall

Nozzle Diameter = 1.5 mm
 Pinhole Camera: $d= 50 \mu\text{m}$
 Filter: $0.2 \mu\text{m}$ of Al on
 $1 \mu\text{m}$ of polycarbonate

Figure 12: Single-exposure x-ray pinhole camera images of Xe(M) radiation $\sim 1 \text{ keV}$ from a stable laser channel in gaseous $(\text{Xe})_n$. The pseudo-color images show longitudinal multi-foci filament structure and evidence of a strong emittance cone highlighted by an arrow-shaped region of ionization in the forward direction exiting the channel. Approximate location of the focal region is indicated along with the corresponding Rayleigh range of the focussing system ($f/3$). Incident 248 nm laser pulse had a duration of $\sim 250 \text{ fs}$, and energy of $\sim 350 \text{ mJ}$. The pinhole camera aperture was $25 \mu\text{m}$ with $M \sim 10$ and a thin kapton filter eliminated optical background.

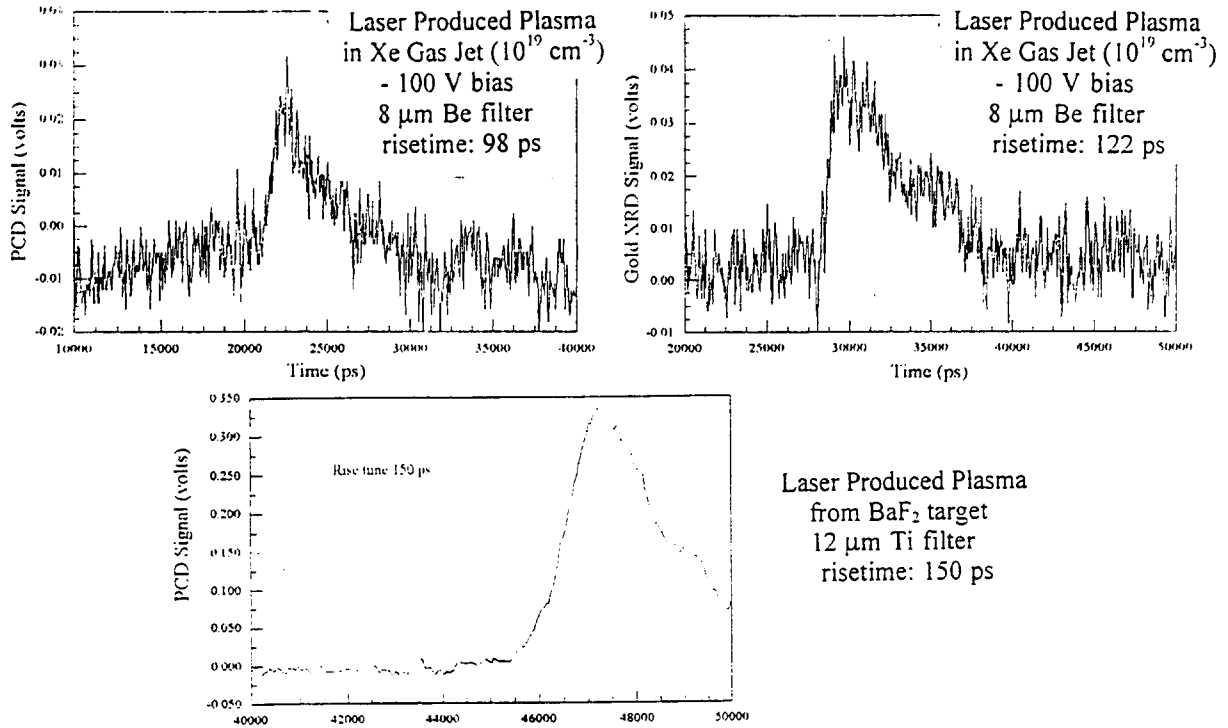


Figure 13: Time-dependent x-ray response signals for XRD and PCD devices excited with Xe(M) and barium fluoride L-shell. The signal is noisier for the case of xenon gas because of the lower gas density.

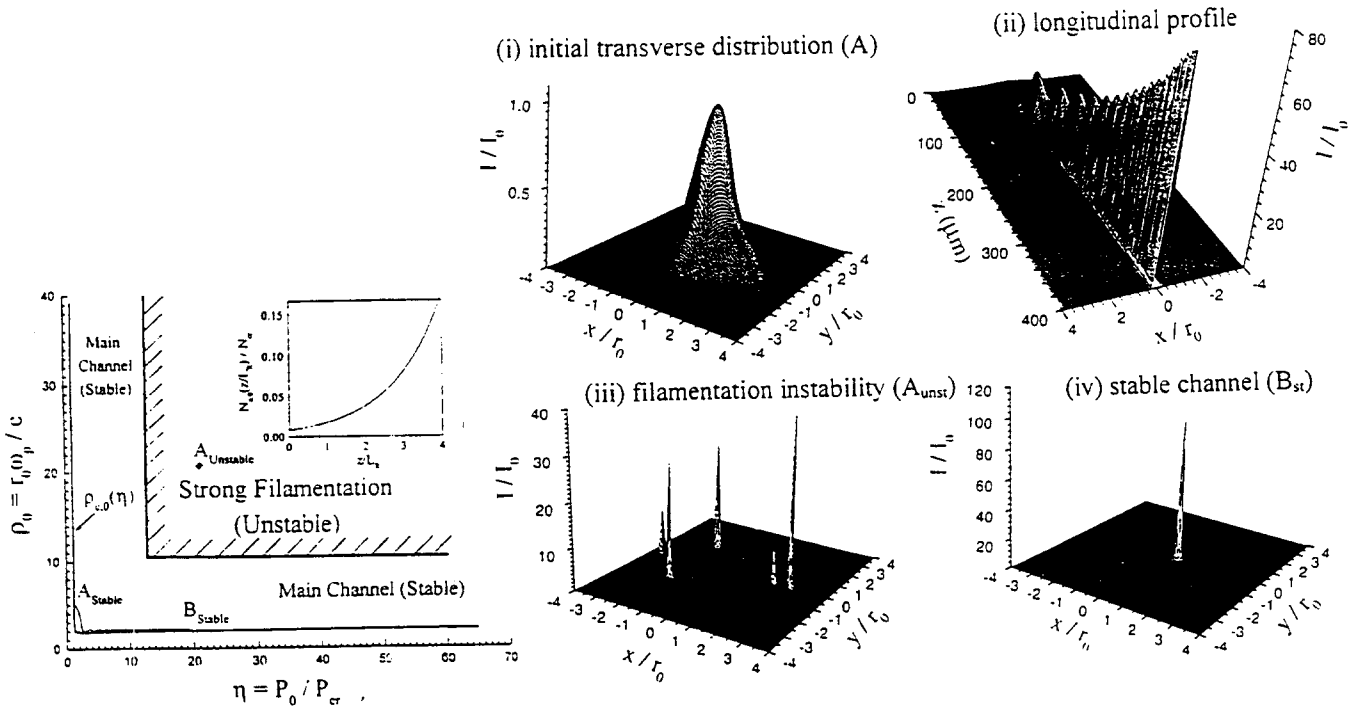


Figure 14: Representative stability map in the η - ρ plane for relativistic and charge displacement self-channeling of Gaussian beams in homogeneous plasma. Evolving longitudinal and transverse intensity distributions along the trajectory path A-B are shown in the insert.

transverse profiles of the laser intensity and plasma electron density are defined by the lowest eigenmodes of the governing NLSE while an unstable propagation dynamic such as filamentation is dominated by the formation of higher-order transverse modes. These stable and unstable regions characteristic of channel formation are best illustrated in the geography of the η - ρ coordinate plane where $\eta=P_o/P_{crit}$ and $\rho=r_o\omega_p/c$ are dimensionless variables related to laser power (relative to critical) and transverse extent, respectively. Using this analytical approach, we can develop a stability map or movie describing the evolution of relativistic and charge displacement channeling of a Gaussian beam in initially homogeneous plasma as shown in figure 14. Starting with the initial normalized intensity distribution $I(x,z)/I_o$, trajectories connecting A_{st} - B_{st} (stable zone) and A_{st} - B_{unst} (unstable zone) can be evaluated to yield the longitudinal development profile and transverse cuts of the self-channeling process. Our solutions confirm that stable axisymmetric modes exist for both the homogeneous plasma case and for the case of a static preformed plasma gradient, or equivalently a azimuthally perturbed pulse.

IV. Applications

• *X-Ray Backlighting/Radiography*

Short-pulse ultrabright x-ray backlighters will be a necessary complement to conventional nanosecond approaches when improved on-axis opacity penetration is required for diagnostic imaging in elevated temperature and density environments exhibiting bright backgrounds such as z-pinch wire array implosions near stagnation or for fuel capsules with high compression ratios. Typically, backlighter energies >10 keV are required to achieve transmission conditions operationally useful for shadowgraphic contrast in these instances. Imploding NIF capsules for example, will feature pusher densities of 700g/cm^3 in $100\ \mu\text{m}$ compressed plasma for a pr of order 1-10; this represents an attenuation factor of $\sim 10^{-22}$ at 6 KeV but only 10^{-2} at 20 KeV (assuming carbon as an absorber and $pr\sim 5$). A short-pulse x-ray source when combined with fast temporal gating would provide improved measurement capability by defeating self-emission of compressed plasma and would enhance image contrast and dynamic range for nondestructive monitoring applications by separating ballistic photons from the scattering photons. For x-ray pulse durations shorter than the typical hydrodynamic timescale, motion is frozen so that increased spatial resolution without penumbral blurring can be achieved allowing high-resolution projection imaging for applications involving detailed structural investigations or rapid dynamical change.

New energetic nonthermal x-ray production mechanisms accessible with laboratory-scale terawatt lasers will facilitate the development of compact drivers with conversion efficiencies $>1\%$ above 10 keV. This conversion can be further improved using high-intensity modes of channeled propagation in combination with short-pulse multiphoton production of x-rays as described previously. Thermal emission from plasmas created by ultrafast lasers and bremsstrahlung from interaction of fast electrons with solid targets can be combined with differential absorption monochromatic imaging in a backlighter geometry to obtain high-contrast and high spatial resolution images of NIF-relevant plasmas, and for radiographic monitoring of weapons components in the stockpile for age-related wear (eg, cracks), fatigue, and corrosion. The small inherent spatial scales and fast timescales have unique advantages for studying radiation-driven shock breakout and the Hugoniot relations for shock compression of materials, time-resolving opacities and mix instabilities, and for precise determination of the spatial scalelength of the electron density gradient or progressive heat flow in an expanding plasma.

The general requirements for an x-ray backlighter are conceptually simple: (1) high spectral

brightness $B = \phi / \Delta A \Delta \Omega \Delta \lambda \Delta \nu$ relative to emission background; (2) capable of penetrating the anticipated opacity conditions with detectable fluence and image contrast; (3) negligible hydrodynamic motion. Based on these basic operational requirements, we attempted to fit together a reasonable spectral intensity model for the Z pulsed power machine over the energy range 100 eV- MeV using the limited PCD and crystal spectrometer data available, and extrapolating (interpolating) sparse or unknown regions using empirical Planckian and Boltzmann models consistent with energy balance. Using our measured experimental conversion efficiency for Au @ 10 keV (~1 %), we then estimated the achievable x-ray spectral radiance using a femtosecond terawatt laser based on CPA hybridization of an existing Nd:glass laser deployed on Z. Our results indicate that such a tabletop backlighter would exceed the requirements.

• *Ultrafast probing of atomic structure*

Recent developments in laser engineering, short-wavelength optics, and the physics of x-ray generation have made possible a new class of materials science experiments in which matter is irradiated with short pulses of laser-driven x-rays synchronized with optical excitation. Such experiments offer unique scientific opportunities for evaluating nonlinear x-ray interaction with bulk matter and surface interfaces, facilitate studies of x-ray stimulated chemistry and electronic desorption, and allow well-established x-ray techniques such as diffraction and edge absorption with their inherent atomic-scale spatial resolution to be performed on a picosecond time resolution relevant to surface dynamics. By spatially delaying part of the laser pulse that activates the x-rays from that which irradiates the sample, a "stroboscopic" diffraction pattern image or snapshot can freeze changes in the transient surface morphology and bond order as a function of time delay. Alternatively, one could directly observe radiation-driven shocks in solid density materials and measure shock position as function of time and material compression using transmission of x-rays.

X-ray diffractometry exploits interference effects created by adjacent atomic planes (Bragg) to obtain global structural information about fluid or crystal samples. Since x-ray diffraction measurements can be directly inverted to obtain atomic position or bond length, it is conceivable that ultrafast exposure with a pump/probe timing configuration could be used to diagnose dynamical processes such as chemical reactions or phase transitions. This method could directly track the melt history of a metal lattice or epitaxial thin film from electron heating through electron-phonon coupling and subsequent disorder and/or recrystallization. Surface temperature and bond changes during the process would be apparent in the transient x-ray diffraction pattern signature. Development of a time-resolved x-ray diffraction system capable of dynamically resolving structural changes induced by an external optical stimulus would significantly contribute to our understanding of basic materials science and materials processing. Applications of this technological approach to flash microradiography and pulsed ionization/radiation damage effects testing in microelectronics and weapons components are also expected. The reduced sample exposure time inherent to a pulsed measurement process offers advantages for biological imaging and x-ray holography of hydrated specimens. Because x-rays can penetrate harsh processing environments, realtime x-ray diffraction and spectroscopy are ideal for analysis during vapor phase materials processing.

Extended x-ray absorption fine structure (EXAFS) gleans information regarding the local neighborhood of a given atom or chemical compound using the K-edge absorption spectrum, notably C(277 eV), N(391 eV), and O(530 eV). The advantage of spectroscopic techniques over diffractometry is that the required x-ray photon flux is several orders of magnitude lower. A major application of short-pulses of bright x-rays in this region will be high contrast

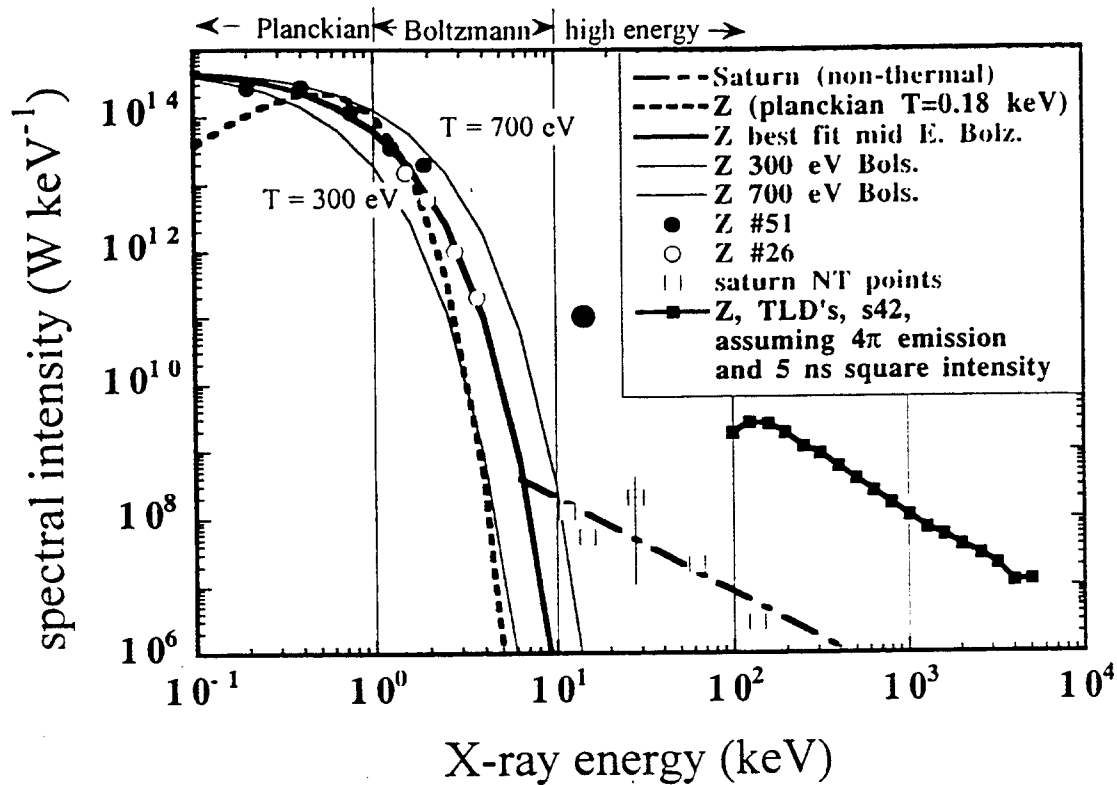
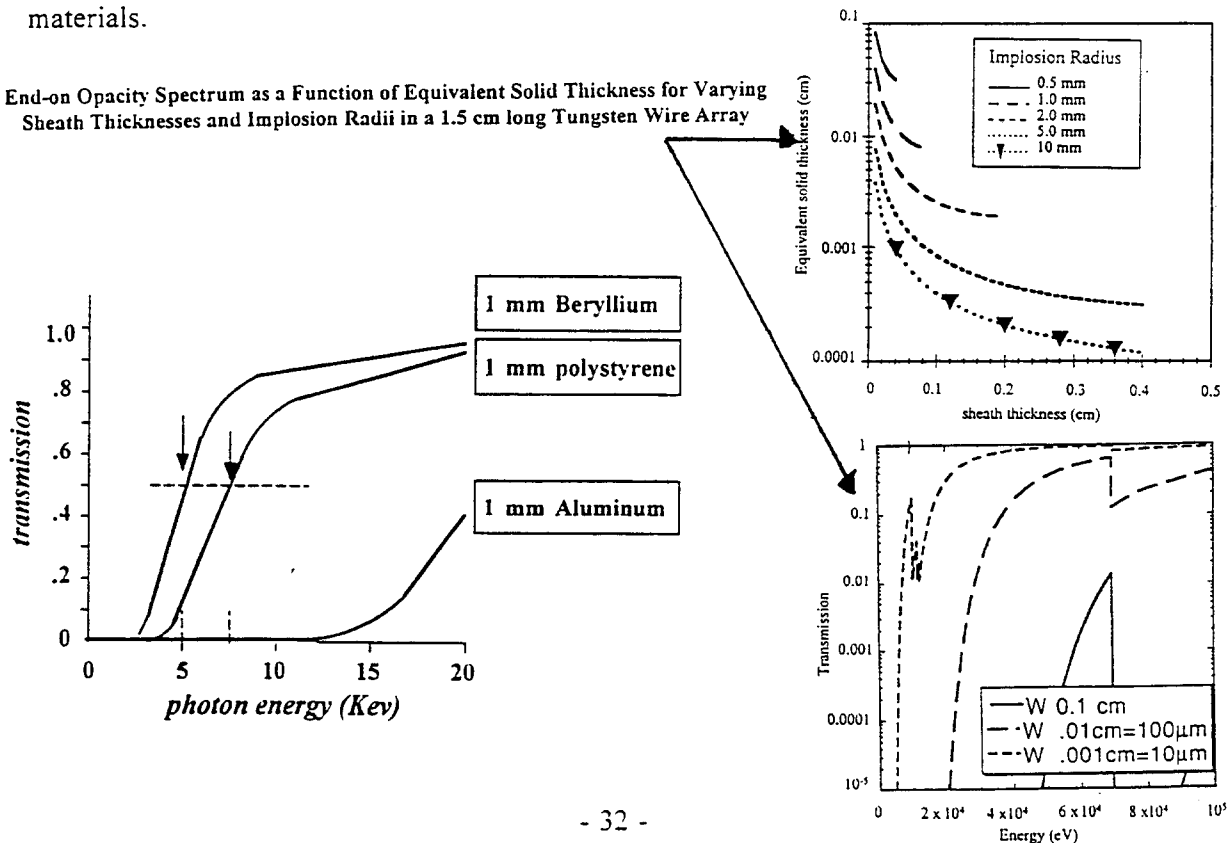


Figure 15: Spectral intensity ($WkeV^{-1}$) of the Z-pulse power machine with a tungsten load as a function of energy in comparison to a 10 joule 450 fs x-ray backlighter using the experimentally established Au target conversion efficiency. Known data and theoretical fit functions for temperature are included for clarity. Onset shows opacity curves for various materials.

End-on Opacity Spectrum as a Function of Equivalent Solid Thickness for Varying Sheath Thicknesses and Implosion Radii in a 1.5 cm long Tungsten Wire Array



absorption imaging of the carbon in proteins and cellular structure relative to the oxygen in water. Harder x-rays near the iodine K-edge ~ 27 keV will be useful for medical differential imaging and angiography. Short-pulse ballistic imaging will improve the resulting image contrast and spatial resolution by eliminating the scattered component. Because of its inherent short wavelength and significant penetration depth, x-ray microscopy is a versatile tool to study structural composition (elemental map).

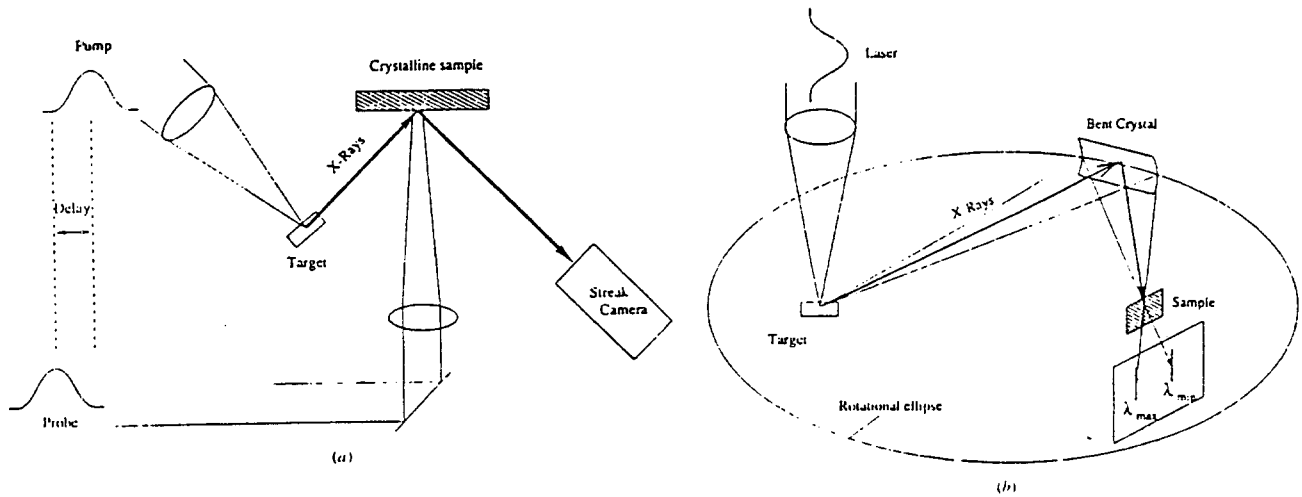


Figure 16: X-ray optical arrangements for (a) pump-probe diffractometry, and (b) ultrafast absorption spectroscopy. [From Gibbon and Forster]

• Laser Wakefield Accelerator

Conventional particle accelerator technologies are limited by electrical breakdown to field gradients of order 100 MeV/m. Recently, there has been a resurgence of interest in collective acceleration using large-amplitude plasma waves because such devices are already ionized and can theoretically support a field with $\times 10^4$ larger gradient over a short length. Studies of electron plasma wave excitation show that it should be possible to obtain 5 GeV energies of accelerated electrons using a multi-terawatt-class Ti:S laser in combination with channeled propagation over a distance of 5 cm and a plasma density of $\sim 10^{18}$ cm $^{-3}$. In this process, the laser pondermotive force combined with ion inertia which provides an electrostatic restoring force can drive a longitudinal electrostatic wakefield or charge density wave at nearly the speed of light, thereby preferentially accelerating electron bunches trapped in the wave along the axial direction of laser propagation to GeV/m. The transverse electromagnetic laser energy is coupled into longitudinal plasma waves (accelerating field E_p is proportional to the epw amplitude) with high phase velocity and effective acceleration length L_a :

$$E_p = m_e c \omega_p / e \sim (N_e / 10^{18} \text{ cm}^{-3})^{1/2} \text{ GV/cm} \quad [4]$$

$$v_{ph} = c \{ 1 - (\omega_p / \omega_0)^2 \}^{1/2}$$

$$L_a = \lambda / [2(c - v_{ph})]$$

Maximum energy gain of the accelerated electrons by the plasma wave becomes $\Delta U = E_p L_a$. As distinguished from the beat wave mechanism which requires a laser heterodyne beat resonant with the plasma, resonant acceleration of Langmuir waves for this case occurs by the seeded onset of a modulational instability ($P > P^{cr}$, $\tau_p > \pi/\omega_p$) in the homogeneous plasma which is provided either by the sharp leading edge of the incident optical pulse or due to steepening of the pulse longitudinal profile during relativistic self-focussing. Accelerator technology for laser-guided electron beams and beam steering concepts require improved theoretical scaling and stability analysis. Beam propagation experiment injecting relativistic e-beams into refractively guided laser ionization channels formed by self-focussing and space-charge expulsion are in their infancy although promising with measured outputs of 1 nC of charge per bunch (MeV) in a low emittance beam (1 mm-mrad). The nonlinear refractive response of the plasma that leads to spatially modified propagation will also give rise to other phenomena such as self-phase modulation which will affect pulse shape and parametric instabilities. New applications such as nonlinear Thomson scattering from SMLWA's and coherent x-ray harmonics generated by relativistic currents generated across an abrupt vacuum-solid interface will likely result from research progress in this direction.

• *Optically induced nuclear fusion*

The process of nuclear fission can be induced by electromagnetic interactions involving photons if sufficient energy can be communicated to the nucleus to enable the system to penetrate the fusion barrier. It has been proposed that driven motions of atomic electrons arising from intense laser irradiation and nonlinear radiative coupling can transfer excitation energy to nuclear transitions. For 248 nm radiation at an intensity of 10^{21} W/cm² highly relativistic currents are produced which can couple to the fission mode of nuclear decay. With irradiation for a time ~100 femtoseconds, calculations indicate a fission probability of 10^{-5} for a U-238 nuclei which is measurable with current generation detectors. Acceleration/generation of relativistic electrons to sufficient energy to surpass the threshold of the fission reaction can be achieved in the focal region of such an intense laser pulse both by electron collision mechanism (electrofission) and by true photofission due to bremsstrahlung produced colaterally by fast electrons in the target material:

$$\text{photofission channel: } \gamma + A \rightarrow f_1 + f_2 + \nu n \quad (\sigma_f) \quad [5]$$

$$\text{electrofission channel: } e^- + A \rightarrow f_1 + f_2 + \nu n + e^- \quad (\sigma_{ef})$$

The threshold electron energy for electrofission ~10 MeV which requires channeled TW or PW-class short-pulse lasers to drive the reaction pathway. Large instantaneous fission rates generated in nuclear materials may be useful for bright and spatially localized high-flux pulsed sources of fission fragments, neutrons, and gamma rays $>10^{24}$ fission frag/cm² s.

• *Fast Igniter*

The concept of fast igniter is intimately connected with the fundamental phenomena of ultra-intense laser light beam propagation through dense matter and seeks to decouple compression uniformity from ignition. For traditional inertial confinement fusion, energies >MJ are needed for significant gain and the implosion symmetry must be controlled better than 1%. In the fast ignitor concept, an intense external short-pulse laser (~10 ps, 10^{20} W/cm²) is focussed on a compressed core to produce isochoric hot-spot ignition. The deuterium-tritium fuel assembly is formed by a conventional ablatively-driven implosion. The optical sparkplug lowers the ignition requirements for ICF by boring through the coronal

plasma due to radiation pressure and delivering energy in the form of fast electrons. There are three actual stages in this scheme (1) first fuel is compressed to a radius ~ 10 microns, the equivalent of alpha particle range at an areal density of $.4 \text{ g/cm}^2$. Next (2) a prepulse several hundred ps long with tailored intensity profile is used to create an optical channel through the underdense corona and push the critical surface inward to target center; finally (3) short intense pulses are sent down the preformed channel to the high-density core where it heats electrons to MeV energies- these fast electrons penetrate the fuel where they thermalize and ultimately heat ions to fusion temperature (5-10 KeV). Magnetic fields are expected to play a significant role in establishing a return current and modifying lateral transport, and need to be evaluated in short-pulse laser channeling experiments.

• *Adaptive optics*

The brightness and ultimate focussed irradiance achievable with a laser pulse is determined by both the peak power and the spatial divergence. Adaptive optics compensation with deformable segmented mirrors and active wavefront sensing technology can dramatically increase the useable focal irradiance and Strehl ratio in the presence of aberrations or distortions. State-of-the-art wavefront control instrumentation can correct for linear and nonlinear aberrations internal to the laser and in beam transport to a level better than $\lambda/10$ rms. By properly accounting for B-integral distortions and diffraction in the chirped pulse amplification process, the spatial intensity distribution can be optimized for channel stability. Dispersion compensation and phase control can be incorporated concurrently using a programmable pulse shaping apparatus in the oscillator to tailor the time-domain characteristics.

• *Recombination X-ray lasers*

The aim of transient recombination x-ray lasers based on field ionization is to achieve a brief population inversion in a cold overionized plasma background which has favorable scaling for magnitude of stimulated emission in comparison with the laser excitation power. For practical implementation to table-top drivers, low electron temperatures at high density are required to minimize collisional excitation and maximize recombination without the accompanying electron heating mechanisms (eg, above threshold ionization, stimulated Raman scattering, and nonlinear inverse bremsstrahlung). Since the number of e-foldings of the SRS instability and the IB heating process both increase with pulse duration for a given intensity, short pulse lasers with short wavelengths are essential to minimize heating. When such lasers are combined with the creation of self-guiding plasma channels, it is possible to establish a new mode for concentrated energy delivery and power compression, which by virtue of creating hollow atoms with core electron vacancies over long refractively-compensated gain scalelengths, can be exploited for efficient x-ray lasing. Improved coupling with the gain medium due to ordered multi-electron motion in the channel will further enhance the lasing process.

• *Electromagnetic pulses*

Self-guided light channeling using focused ultrashort pulses can produce a propagating electrostatic wakefield as result of pondermotively induced charge displacement nonlinearities. In this physical description, oscillating electrons along the ionization channel can be trapped and accelerated in a dynamic space-charge gradient by the wakefield to produce a moving dipole field which travels with the optical pulse. This mechanism can produce a wide-bandwidth electromagnetic current pulse analogous to the Compton flux of recoil electrons. The resulting electromagnetic transient should be highly directional along

the channel propagation axis and correlated with the production of strong bremsstrahlung x-ray emission. A multi-megagauss toroidal B-field is expected near the edge of the focal spot.

V. Conclusion

This report has reviewed the results of an experimental program to understand self-channeled laser propagation in ionized underdense plasmas with femtosecond terawatt lasers. Although extremely promising for the control of hard x-ray production and atomic coupling, more detailed experiments investigating the complex nonlinear interplay between relativistic self-focussing interactions and refractive guiding are necessary to assess the viability of this innovative technology for applications requiring power compression over extended distances including advanced fusion schemes, x-ray lasers, photofission, and electron acceleration. Improved knowledge of the parameter space governing the interactions will benefit their utilization for probing hot-dense matter.

VI. References

- S.C. Wilks and W.L. Kruer, "*Absorption of Ultra-intense Light by Solids and Overdense Plasmas*," IEEE Journal of Quantum Electronics, vol. 33, p. 1954, 1997.
- J.D. Kmetec, C.L. Gordon, J.J. Macklin, B.E. Lemoff, G.S. Brown, and S.E. Harris, "*MeV X-Ray Generation with a Femtosecond Laser*," Phys. Rev. Lett., vol. 68, p. 1527, 1992.
- D. Umstadter, J. Workman, A. Maksimchuk, X. Liu, U. Ellenberger, J.S. Coe, and C.-Y. Chien, "*Picosecond X-rays from Subpicosecond Laser-Produced Hot-Dense Matter*," J. Quant. Spectrosc. Radiat. Transfer, vol. 54, 401, 1995.
- P. Sprangle and E. Esarey, "*Interaction of Ultrahigh Laser Fields with Beams and Particles*," Phys. Fluids B, vol. 4, p. 22411, 1992.
- P. Gibbon and E. Forster, "*Short-Pulse Laser-Plasma Interactions*," Plasma Phys. Control. Fusion, vol. 38, 769, 1996.
- F.N. Beg, A.R. Bell, A.E. Dangor, C.N. Danson, A.P. Fews, M.E. Glinsky, B.A. Hammel, P. Lee, P.A. Norreys, and M. Tatarakis, "*A Study of Picosecond Laser-Solid Interactions Up to $10^{19} \text{ W cm}^{-2}$* ," Phys. Plasmas, vol. 4, p. 447, 1997.
- E. Esarey, "*Short Laser Pulses in Ionizing Gases and Plasmas*," IEEE J. Quant. Elec., vol. 33, p. 1907, 1997. (and references therein)
- A. Ting, K. Krushelnick, C.I. Moore, H.R. Burris, E. Esarey, J. Krall, and P. Sprangle, "*Temporal Evolution of Self-Modulated Laser Wakefields Measured by Coherent Thomson Scattering*," Phys. Rev. Lett., vol. 77, p. 5377, 1996.
- J. Workman, A. Maksimchuk, X. Liu, U. Ellenberger, J.S. Coe, C.-Y. Chien, and D. Umstadter, "*Control of Bright Picosecond X-Ray Emission from Intense Subpicosecond Laser-Plasma Interactions*," Phys. Rev. Lett., vol. 75, p. 2324, 1995.
- C.W. Siders, S.P. Le Blanc, D. Fisher, T. Tajima, and M. Downer, "*Laser Wakefield Excitation and Measurement by Femtosecond Longitudinal Interferometry*," Phys. Rev. Lett., vol. 76, p. 3570, 1996.
- R. Wagner, S.-Y. Chen, A. Maksimchuk, and D. Umstadter, "*Electron Acceleration by a Laser Wakefield in a Relativistically Self-Guided Channel*," Phys. Rev. Lett., vol. 78, p. 3125, 1997.
- A.B. Borisov, X. Shi, V.B. Karpov, V.V. Korobkin, J.C. Solem, O.B. Shiryayev, A. McPherson, K. Boyer, and C.K. Rhodes, "*Stable Self-Channeling of Intense Ultraviolet Pulses in Underdense Plasma, Producing Channels Exceeding 100 Rayleigh Lengths*," J. Opt. Soc. Am. B, vol. 11, p. 1941, 1994.
- A.B. Borisov, O.B. Shiryayev, A. McPherson, K. Boyer, and C.K. Rhodes, "*Stability Analysis of Relativistic and Charge-Displacement Self-Channeling of Intense Laser Pulses in Underdense Plasmas*," Plasma Phys. Control. Fusion, vol. 37, p. 569, 1995.
- F. Druon, G. Cheriaux, J. Faure, J. Nees, M. Nantel, A. Maksimchuk, and G. Mourou, "*Wave-front Correction of Femtosecond Terawatt Lasers by Deformable Mirrors*," Optics Lett., vol. 23, p. 1043, 1998.

Publications Generated from this Work:

A.B. Borisov, J.W. Longworth, K. Boyer, C.K. Rhodes, "*Stable Relativistic/charge displacement channels in ultrahigh power density plasmas,*" Proc. Natl. Acad. Sci. Vol.95(June1998)

S.M. Cameron, D.E. Bliss, C.K. Rhodes, *Self-Guided Laser Optical Channeling in Air with High-Intensity Ultrashort Pulses: Applications to Remote Sensing*" Presented at International Workshop on Ultrafast Intense Laser Pulse Propagation and Its Applications, June 1998 Laval University, Quebec City Quebec

Stable relativistic/charge-displacement channels in ultrahigh power density ($\approx 10^{21}$ W/cm³) plasmas

A. B. BORISOV*†, J. W. LONGWORTH*‡, K. BOYER*, AND C. K. RHODES*†§

*Department of Physics (M/C 273), University of Illinois, 845 West Taylor Street, Chicago, IL 60607-7059; †Center for Tsukuba Advanced Research Alliance (TARA), University of Tsukuba, 1-1-1 Tennodai, Tsukuba, Ibaraki 305, Japan; and ‡Department of Physics, Illinois Institute of Technology, Chicago, IL 60616

Stable relativistic/charge-displacement channels in ultrahigh power density ($\approx 10^{21}$ W/cm³) plasmas

A. B. BORISOV*†, J. W. LONGWORTH*‡, K. BOYER*, AND C. K. RHODES*†§

*Department of Physics (M/C 273), University of Illinois, 845 West Taylor Street, Chicago, IL 60607-7059; †Center for Tsukuba Advanced Research Alliance (TARA), University of Tsukuba, 1-1-1 Tennodai, Tsukuba, Ibaraki 305, Japan; and ‡Department of Physics, Illinois Institute of Technology, Chicago, IL 60616

Communicated by Charles H. Townes, University of California, Berkeley, CA, May 8, 1998 (received for review February 27, 1998)

ABSTRACT Robust stability is a chief characteristic of relativistic/charge-displacement self-channeling. Theoretical analysis of the dynamics of this stability (i) reveals a leading role for the eigenmodes in the development of stable channels, (ii) suggests a technique using a simple longitudinal gradient in the electron density to extend the zone of stability into the high electron density/high power density regime, (iii) indicates that a situation approaching unconditional stability can be achieved, (iv) demonstrates the efficacy of the stable dynamics in trapping severely perturbed beams in single uniform channels, and (v) predicts that $\approx 10^4$ critical powers can be trapped in a single stable channel. The scaling of the maximum power density with the propagating wavelength λ is shown to be proportional to λ^{-4} for a given propagating power and a fixed ratio of the electron plasma density to the critical plasma density. An estimate of the maximum power density that can be achieved in these channels with a power of ≈ 2 TW at a UV (248 nm) wavelength gives a value of $\approx 10^{21}$ W/cm³ with a corresponding atomic specific magnitude of ≈ 60 W/atom. The characteristic intensity propagating in the channel under these conditions exceeds 10^{21} W/cm².

The development of methods for the compression of power in materials is one of the oldest endeavors of mankind with an origin that predates the Stone Age. From the use of a wooden club to the contemporary production of vigorous thermonuclear environments, the achievable power density (W/cm³) has been advanced by approximately a factor of 20 orders of magnitude ($\approx 10^{20}$). New processes, involving the nonlinear interaction of intense ($\approx 10^{18}$ – 10^{21} W/cm²) fs pulses of radiation with matter, currently are being explored to enhance further the controlled production of these environments to a new ultrahigh level ($\approx 10^{19}$ – 10^{21} W/cm³), a range that can approach ≈ 100 W/atom. These conditions provide new possibilities for the production and regulation of many highly energetic physical processes, including hard x-ray generation, the initiation of nuclear reactions, particle acceleration, and the fast ignition of fusion targets. The key to the production of these exceptional conditions is the stable compression of the spatial distribution of powerful ($P_0 \approx 1$ TW–1 PW) pulses of radiation into very narrow plasma channels. Specifically, a complex mechanism, which is triggered by pulses whose power exceeds a critical value P_{cr} and involves both relativistic electron motions and the relative spatial separation of the electron and ion densities caused by the radiation pressure of the intense wave, produces the conditions necessary for channel formation. In brief (1), the ponderomotive radial displacement of the electrons and the contrasting inertial confinement of the ions cooperate to produce the two chief characteristics of the channels. They are (i) the refractive self-focusing action

of the displaced electrons, which confines the propagating radiation, and (ii) the high spatial stability of the channels, the feature produced by the immobile electrostatic spine formed by the fixed ions. These narrow channels, which typically have a diameter of a few microns, represent an example of a new, largely unexplored class of strongly nonequilibrium excited matter that combines a very high energy density with a well-ordered structure.

The existence of dynamic stability is essential for the control of high power density plasmas. Of particular importance are the physical limits of stable behavior and the corresponding implications on the maximum achievable power density. The overall result of this study is that exceptionally robust stability is a chief characteristic of the relativistic, charge-displacement self-channeling mechanism. Specifically, the six key findings are: (i) the discovery of the leading role played by the eigenmodes in the development of stable channels, (ii) the evaluation of a simple technique using a longitudinal gradient in the electron density to extend the zone of stability into the high electron density/high power density regime, (iii) the indication that a situation approaching unconditional stability can be achieved, an outcome reflecting the well-ordered structure of the excited plasma, (iv) the demonstration of the efficacy of the dynamics in efficiently trapping severely spatially perturbed beams in single uniform channels, (v) an estimate showing that an extraordinary power density ($\approx 10^{21}$ W/cm³) can be produced in the channels with UV radiation, and (vi) the prediction that $\approx 10^4$ critical powers (P_{cr}) can be trapped in a single stable channel.

Theoretical work (1) has predicted that the channeled propagation can exhibit a large domain of stability. Initial experimental studies (2–5), conducted close to the threshold condition of the channeling phenomenon (6–15), have furnished evidence supporting this conclusion. Measurements of the spatial properties of the propagation, using both x-ray (4) and Thomson (16, 17) images, have clearly established the formation of long channels of the form shown in Fig. 1. Fig. 1 illustrates a single-exposure x-ray [Xe(M), ≈ 1 keV] image of the longest channel (>50 Rayleigh ranges) that was experimentally produced in a gaseous target containing (Xe)_n clusters (18) with a fs (≈ 250 fs) UV (248 nm) pulse (19) having a peak power of ≈ 1.4 TW. The salient characteristic of the image is a long, stable, and uniform channel of high power density, the magnitude (20) of which was estimated to be $\approx 2 \times 10^{19}$ W/cm², or equivalently ≈ 1 W/atom. Other work (17), which examined the channeled region with images of the Thomson scattered 248 nm radiation, complemented the data shown in Fig. 1 and demonstrated that the channeling mechanism efficiently compresses the incident power into a single filament whose diameter does not exceed the resolution of the imaging system (5–6 μ m), a result consistent with the corresponding theoretical (2, 4, 12) figure of ≈ 1 –2 μ m. The principal issues discussed herein are the determination of the conditions

The publication costs of this article were defrayed in part by page charge payment. This article must therefore be hereby marked "advertisement" in accordance with 18 U.S.C. §1734 solely to indicate this fact.

© 1998 by The National Academy of Sciences 0027-8424/98/957854-6\$2.00/0
PNAS is available online at <http://www.pnas.org>.

§To whom reprint requests should be addressed. e-mail: rhodes@uic.edu.

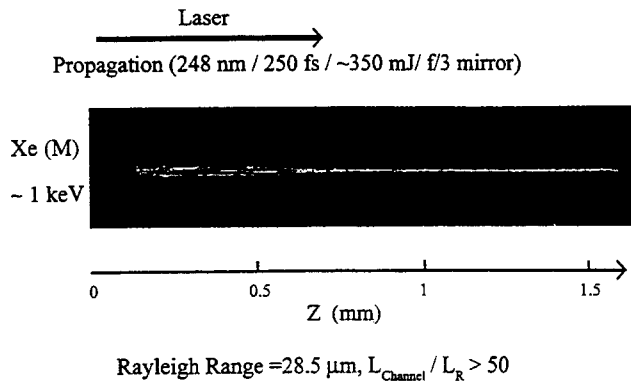


FIG. 1. Single-exposure x-ray image of a stable slender channel emitting Xe(M) radiation (≈ 1 keV) produced in a gaseous target containing $(\text{Xe})_n$ clusters. The incident 248-nm pulse had a duration of ≈ 250 fs and an energy of ≈ 350 mJ, and was focused with f/3 off-axis parabolic mirror. The image was recorded with an x-ray pinhole camera having an aperture with a diameter of $25 \mu\text{m}$ and a spatial resolution of $\approx 30 \mu\text{m}$. Because the Rayleigh length of the focusing system is $28.5 \mu\text{m}$, the observed length of the channel exceeds 50 Rayleigh ranges. Additional experimental details are reported in ref. 4. The color scale (in arbitrary units) of the measured x-ray intensity is defined by black, zero; red through violet, ascending intensity; and white, maximum.

limiting the stability of the confined propagation illustrated in Fig. 1, and the evaluation of the corresponding upper bound on the power density.

Following conventional notation (1), we introduce the definitions of the coordinates of the η - ρ_0 plane given by

$$\eta = P_0/P_{cr}, \quad \rho_0 = r_0\omega_{p,0}/c, \quad [1]$$

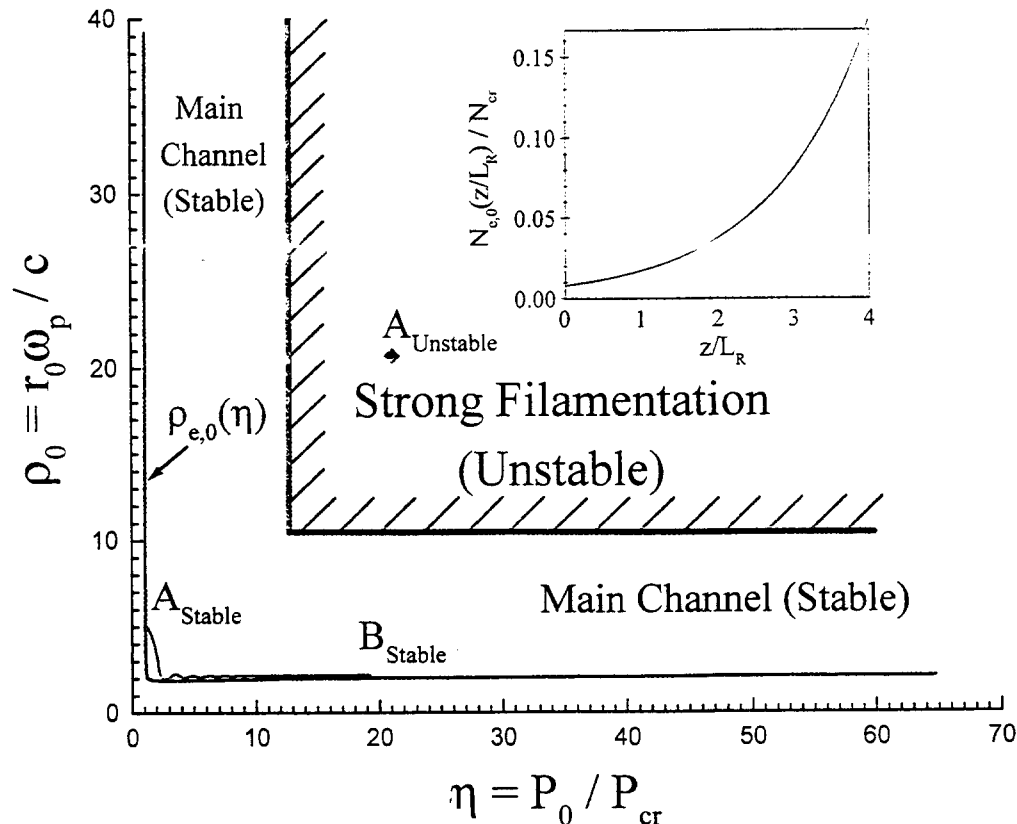


FIG. 2. Stability map in the η - ρ_0 plane for relativistic and charge-displacement self-channeling of Gaussian beams in initially homogeneous plasmas. The dimensionless coordinates ρ_0 and η are defined by Eq. 1. Stable and unstable regions in plane (η, ρ_0) and the locus $\rho_{e,0}(\eta)$ for the lowest eigenmodes are shown. Point $A_{UNSTABLE}$ (21.1, 20.6) corresponds to the input pulse shown in Fig. 3A. Points A_{STABLE} and B_{STABLE} and the trajectory connecting them are described in the text. B_{STABLE} corresponds to the intensity distribution given in Fig. 3C. (Inset) The exponential longitudinal (z) electron density profile $[N_{e,0}(z) = N_{e,0}(0)\exp(\alpha z), N_{e,0}(z = 3.95 L_R) = 20 N_{e,0}(0) = 1/6 N_{cr}]$ between points A_{STABLE} and B_{STABLE} , and L_R denotes the Rayleigh range.

with P_0 denoting the incident peak power and with the critical power (P_{cr}) given by (1, 12)

$$P_{cr} = (m_{e,0}^2 c^5 / e^2) \int_0^\infty g_0^2(\rho) \rho d\rho (\omega / \omega_{p,0})^2 \\ = 1.6198 \times 10^{10} (\omega / \omega_{p,0})^2 W, \quad [2]$$

in which $m_{e,0}$, c , and e have their customary identifications, $g_0(\rho)$ is the Townes mode (21), and ω , $\omega_{p,0}$, and r_0 , are the angular frequency corresponding to the propagating radiation, the angular frequency of the unperturbed plasma, and the radius of the incident intensity profile, respectively. In addition, lowest eigenmodes (1, 10, 12) exist with the dimensionless radius

$$\rho_{e,0} = \left[2 \int_0^\infty U_{s,0}^2(\rho) \rho d\rho / U_{s,0}^2(0) \right]^{1/2}, \quad [3]$$

in which $U_{s,0}(\rho)$ represents the eigenmode (1, 10, 12) with index s . The present analysis was confined to electron densities N_e less than one-quarter of the critical electron density (N_{cr}) to eliminate resonant plasma wave production, and forward Raman scattering (22, 23) was not included, because it is known experimentally that it can be suppressed (24).

Fig. 2 illustrates the geography in the η - ρ_0 plane of the stable and unstable regions characteristic of channel formation in initially homogeneous plasmas (1). The essential features are the locus of the eigenmode curve $\rho_{e,0}(\eta)$ defined by Eq. 3, the existence of a region of stable propagation that includes the

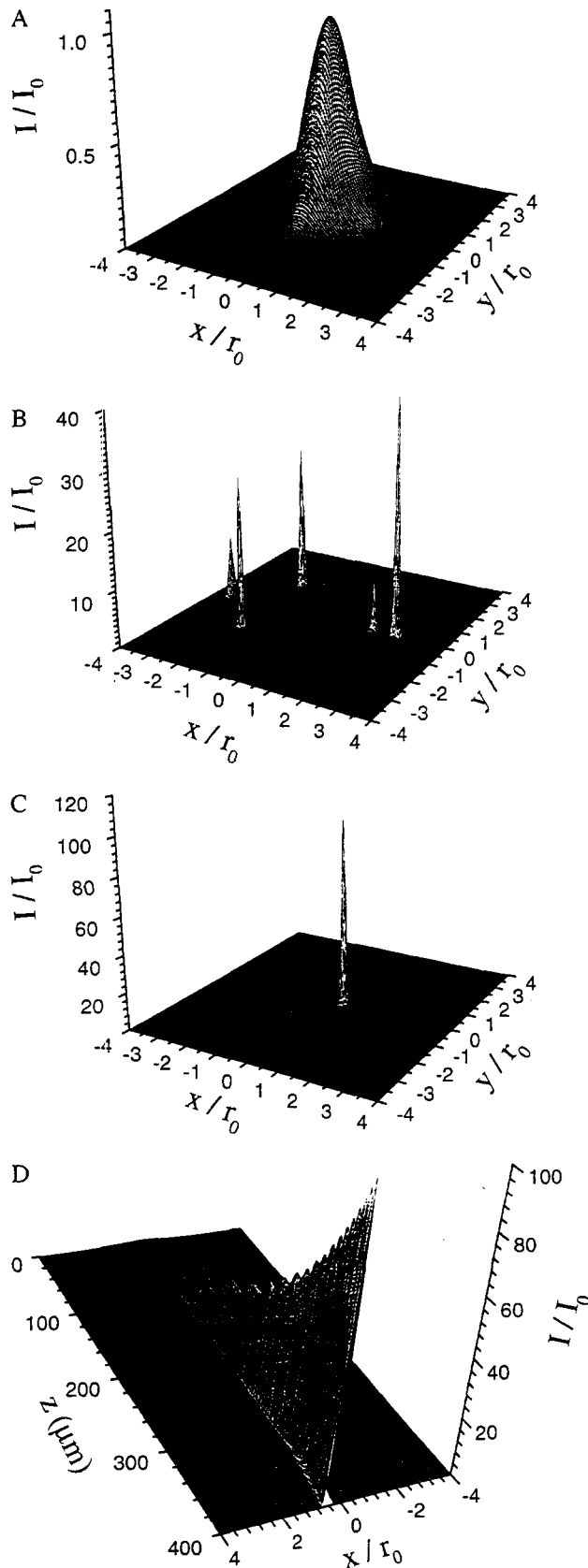


FIG. 3. Propagation characteristics of azimuthally perturbed 2 TW UV ($\lambda = 248$ nm) pulse with the parameters corresponding to data presented in Fig. 2. (A) The initial transverse intensity distribution ($z = 0$) corresponding to point A_{UNSTABLE} in Fig. 2. The azimuthally perturbed Gaussian amplitude distribution has the form $U_0(r, \phi) = I_0^{1/2} \exp(-0.5(r/r_0)^2) \times (1 + (r/r_0)^4 \Sigma \varepsilon_q \cos(q\phi))$. The distribution contains a weak azimuthal perturbation characterized by $\varepsilon_q = 0.03$, $q = 1-4$, and $\delta_{\text{int}} = \max |U_0(r, \phi_1) - U_0(r, \phi_2)|/I_0 = 0.21$. The laser pulse and plasma parameters are

eigenmode curve, and a large zone of unstable propagation involving strong filamentation.

To increase the power density (W/cm^2) in the channel, both high electron density (N_e) and high radiative intensity (I) must simultaneously exist. This condition, which can be achieved by raising both the electron density (N_e) and the power (P_0) propagating in the channel, has the direct consequence of a correlated increase in both ρ_0 and η , a trend that naturally displaces the operating point of the system directly toward and eventually into the unstable zone. Therefore, the attempt to increase the power density in this straightforward manner is immediately blocked by the onset of unstable plasma dynamics. However, this limitation is overcome if there exists a mechanism maintaining the location of the operating point in the stable zone regardless of the fact that sufficiently high values of η and N_e normally exhibit unstable behavior. Analysis described below indicates that the use of an appropriate longitudinal (z) electron density gradient can achieve this goal, thereby, simply and effectively providing a large extension of the zone of stability and a corresponding major increase in the power density. Moreover, it is found that the electron density profile can be arranged in such a way that the locus of the operating point of the system becomes dynamically trapped in the stable zone by the rapid adjustment of the system to a neighborhood close to the eigenmode curve. Therefore, if the initial condition corresponds to stability, the strong dynamical preference for the eigenmode isolates the system in the stable region and the trajectory of the operating point is prevented from entering the unstable zone.

The results shown in Figs. 2–4 both illustrate the details of the propagation and provide a basis for estimating the corresponding bound on the power density. Fig. 3A presents an initial ($z = 0$) transverse intensity distribution that corresponds to point A_{UNSTABLE} ($\eta = 21.1$, $\rho_0 = 20.6$) in Fig. 2. Because this condition falls well within the unstable zone, the beam develops rapidly ($z = 400 \mu\text{m} = 3.95 L_R$, $L_R \equiv$ Rayleigh range) into the fragmented multichannel form shown in Fig. 3B.

The use of an appropriate longitudinal electron density profile, such as that given in the inset of Fig. 2, can be used to achieve the stable propagation depicted in Fig. 3C at both the high electron density and incident power associated with point A_{UNSTABLE} given in Fig. 2. Basically, the use of the longitudinal electron density profile shown in the inset of Fig. 2 maps the point A_{UNSTABLE} to the point A_{STABLE} in the stable zone of Fig. 2, thereby enabling the system to evolve to B_{STABLE} , the point corresponding to the intensity distribution shown in Fig. 3C. The profile of the pulse, as it evolves from A_{STABLE} to B_{STABLE} , is illustrated in Fig. 3D.

$\lambda = 248$ nm, $P_0 = 2$ TW, $r_0 = 2 \mu\text{m}$, $I_0 = 1.59 \times 10^{19}$ W/cm 2 , $N_{e,0} = 3.0 \times 10^{21}$ cm $^{-3}$ ($N_{e,0}/N_{cr} = 1/6$), $\eta(0) = 21.1$, $\rho(0) = 20.6$. (B) Multifocal filamentation arising from unstable propagation originating from point A_{UNSTABLE} in the case of initially uniform longitudinal electron density profile ($N_{e,0} = 3.0 \times 10^{21}$ cm $^{-3} \equiv \text{const}$) with the initial transverse intensity distribution illustrated in A. The corresponding longitudinal position is $z = 3.95 L_R = 400 \mu\text{m}$ and $I_0 = 1.59 \times 10^{19}$ W/cm 2 . (C) Transverse intensity distribution of the stable channel corresponding to point B_{STABLE} in Fig. 2. The channel forms from the initial transverse intensity distribution shown in A in an underdense plasma with the exponential longitudinal electron density profile depicted in the inset of Fig. 2. The longitudinal position is $z_B = 3.95 L_R = 400 \mu\text{m}$ and $I_0 = 1.59 \times 10^{19}$ W/cm 2 . The parameters of the exponential longitudinal electron density profile are: $N_{e,0}(0) = 1.5 \times 10^{20}$ cm $^{-3}$ and $N_{e,0}(z_B) = 3.0 \times 10^{21}$ cm $^{-3} = 1/6 N_{cr}$. The peak intensity in the channel is $I_{\text{ch}} = 1.62 \times 10^{21}$ W/cm 2 . C illustrates the transverse profile of the evolved form. (D) Longitudinal development profile of the stable channel during evolution along the trajectory connecting A_{STABLE} and B_{STABLE} in Fig. 2. The normalized $I(x,z)/I_0$ laser intensity distribution is shown. Coordinate z represents the direction of propagation and x is one of the transverse coordinates. A single high power density channel is formed.

The remapping of the initial condition fundamentally alters the dynamics of the propagation. In the comparison of Fig. 3 *B* and *C*, the strongly unstable propagation in Fig. 3*B* is converted into the formation of a single stable channel that contains more than 85% of the incident power. This dramatic shift in the behavior is driven by the dynamics of the stable region, namely, the strong proclivity of the system to seek the lowest eigenmode. This characteristic of the dynamics is clearly illustrated in the form of the trajectory of the operating point in Fig. 2, which connects the initial conditions corresponding to point A_{STABLE} with the final evolved channel denoted by datum B_{STABLE} . The path of this trajectory demonstrates emphatically that the system aggressively moves toward the eigenmode and remains virtually locked in a small neighborhood of the eigenmode curve as the electron density (N_e) and corresponding value of η both rise to the conditions of high power density. This dynamical behavior contrasts sharply with other mechanisms of self-focusing (e.g., Kerr and relativistic), which generally manifest very poor characteristics of stability (11, 25, 26).

The powerful tendency for attraction to the eigenmode, illustrated by the trajectory pictured in Fig. 2, suggests that the confined propagation may be highly robust against large spatial perturbations of the incident intensity profile. To evaluate this possibility, particularly for high power (\gg TW) infrared ($\lambda = 1 \mu\text{m}$) pulses, the severely azimuthally aberrated intensity distribution of a 1 PW pulse shown in Fig. 4*A* was used to replace the weakly aberrated counterpart presented in Fig. 3*A*. The corresponding results are presented in Fig. 4*B–D*. With the initial condition given by point A_{UNSTABLE} in Fig. 4*B*, the expected filamentation rapidly develops. However, the remapping of the launching point of the wave from A_{UNSTABLE} to A_{STABLE} with the longitudinal electron density profile depicted in the inset of Fig. 2 fully restores the stable pattern of propagation as illustrated in Fig. 4*C*. The corresponding trajectory of the operating point arising from the initial condition A_{STABLE} is illustrated in Fig. 4*B*. We note again the rapid convergence of the eigenmode curve and the efficient achievement of a single channel with the high power density corresponding to B_{STABLE} , a point representing a stable chan-

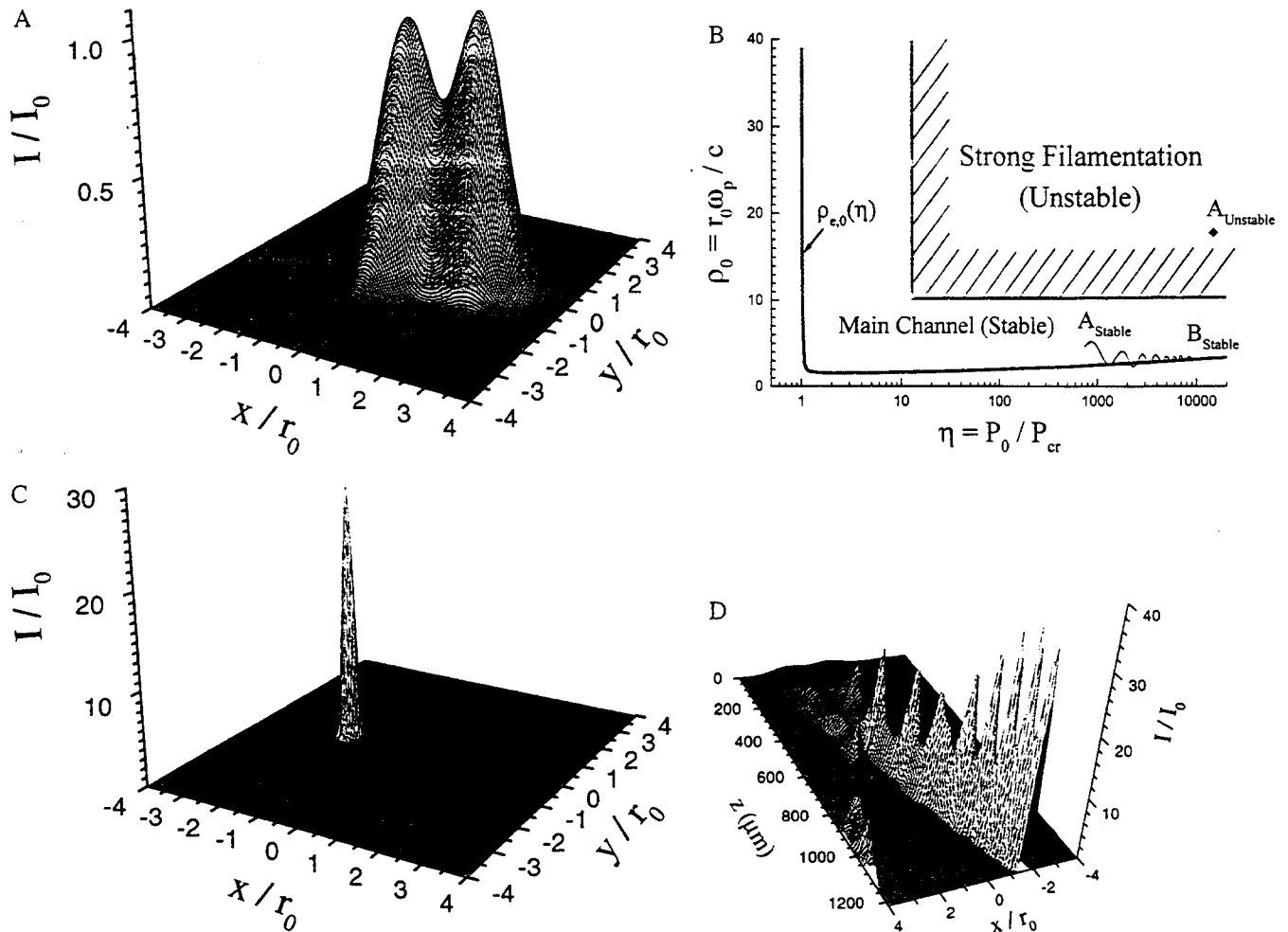


FIG. 4. Propagation characteristics of strongly azimuthally perturbed 1 PW infrared ($\lambda = 1 \mu\text{m}$) pulse. (A) Initial ($z = 0$) transverse (x, y) intensity distribution corresponding to point A_{STABLE} in *B*. The azimuthally perturbed Gaussian amplitude distribution has the form $U_0(r, \phi) = I_0^{1/2} \exp(-0.5(r/r_0)^2) \times (1 + (r/r_0)^2 \sum_{q=1}^4 \epsilon_q \cos(q\phi))$. The distribution involves a gross azimuthal perturbation characterized by $\epsilon_q = 0.1$, $q = 1-4$, and $\delta_{\text{int}} = \max |I_0(r, \phi_1) - I_0(r, \phi_2)|/I_0 = 1.06$. The laser pulse and plasma parameters are $P_0 = 1 \text{ PW}$, $\lambda = 1 \mu\text{m}$, $r_0 = 7 \mu\text{m}$, $I_0 = 6.5 \times 10^{20} \text{ W/cm}^2$, $N_{e,0}(0) = 9.23 \times 10^{18} \text{ cm}^{-3}$, $\eta(0) = 749$, $\rho(0) = 4.72$. (B) Stability map in the η - ρ_0 plane that displays data corresponding to the propagation of the aberrated 1 PW, $\lambda = 1 \mu\text{m}$ pulse. See text for details. (C) Transverse (x, y) intensity distribution corresponding to point B_{STABLE} in *B* showing the formation of a stable single channel. The channel forms from the initial transverse intensity distribution is shown in *A* in underdense plasma with the exponential longitudinal electron density profile depicted in the inset of Fig. 2. The longitudinal position is $z_B = 3.95 L_R = 1215.2 \mu\text{m}$, the incident peak intensity is $I_0 = 6.5 \times 10^{20} \text{ W/cm}^2$, and the corresponding electron density is $N_{e,0}(z_B) = 1.85 \times 10^{20} \text{ cm}^{-3}$, $[N_{e,0}(z_B)/N_{cr} = 1/6]$. The maximum intensity in the channel is $I_{\text{ch}} = 2.5 \times 10^{22} \text{ W/cm}^2$. *C* illustrates the transverse profile of the evolved form. (D) Longitudinal development profile of the stable channel during evolution along the trajectory connecting A_{STABLE} and B_{STABLE} in *B*. The normalized $I(x, z)/I_0$ laser intensity distribution is shown. Coordinate z represents the direction of propagation and x is one of the transverse coordinates.

nel containing approximately 10^4 critical powers. It is significant that the gross spatial restructuring of the pulse shown in Fig. 4D occurs with a modest loss of power, in this case, about 30%. The exceptional stability demonstrated by this result indicates that incident beam profiles deviating greatly from ideal spatial form can be efficiently converted into high brightness configurations.

The results discussed above provide the basis for an estimate of the upper bound of the controlled power density that can be achieved and the dependence of that limit on the wavelength (λ) of the propagating radiation. For $\lambda = 248$ nm, $N_e/N_{cr} \cong 1/6$, and an incident $P_0 = 2$ TW, it was found (cf. Fig. 3C) that the peak intensity in the channel is $I_{ch} \cong 1.62 \times 10^{21}$ W/cm². To estimate the effective cross section σ_{ny} for coupling of the radiation to the atomic or molecular material in the channel, we use a previous estimate (27) of the upper bound of σ_{ny} valid in the limit of sufficiently high intensity ($>10^{20}$ W/cm²) and sufficiently high atomic number (Z). This analysis (27) led to a universal magnitude given by $\sigma_{ny} = 8\pi\lambda_c^2$ in which λ_c is the Compton wavelength of the electron. In arriving at this value for σ_{ny} , appeal was made to a picture involving an extreme form of ordered driven electronic motion in atoms (28), a model that bears an analogy to certain atom-atom and ion-atom collisional processes (29). We note that this value of σ_{ny} also has an experimental basis, because it gives good agreement (20) for power densities (≈ 1 W/atom) derived from images of Xe x-ray spectra produced in channels (30, 31). If we further assume that the channel contains uranium atoms at an average density N_U that experience ionization to the level $Z = 70$, the state of ionization predicted at an intensity $\approx 1.7 \times 10^{21}$ W/cm² by the Coulomb suppression model (32), we can write the corresponding power density (P/V) approximately as

$$\frac{P}{V} \cong N_U \sigma_{ny} I = \frac{N_e}{Z} \sigma_{ny} I \cong 2.6 \times 10^{21} \text{ W/cm}^3, \quad [4]$$

or equivalently ≈ 60 W/atom.

Because the self-channeling causes the transverse intensity profile of the laser beam to stabilize near a lowest eigenmode (1, 3, 12), the peak intensity I_{ch} in the channel can be expressed from Eqs. 1–3 as (1, 4)

$$I_{ch} = \left(\frac{4\pi\eta_{ch}}{\rho_{e,0}} \right) \left(\frac{m_{e,0}^2 c^5}{e^2 \lambda^2} \right) \int_0^\infty g_0^2(\rho) \rho d\rho, \quad [5]$$

where $\eta_{ch} = P_{ch}/P_{cr}$, and P_{ch} represents the power trapped in the channel. For the range of $1.4 \leq \eta_{ch} \leq 10$, the normalized radius of the lowest eigenmodes is nearly constant (1, 3), $\rho_{e,0} \cong 1.7$, and Eq. 5 reduces to the simple expression

$$I_{ch} = 7 \times 10^{18} \frac{\eta_{ch}}{\lambda^2} \text{ W/cm}^2 \quad [6]$$

with λ given in units of micrometers.

The self-channeling of ultra-powerful PW laser pulses in high density plasmas generally involves a trapped power in the channel P_{ch} that is the order of 10^3 – $10^4 P_{cr}$. For this range ($10^3 \leq \eta_{ch} \leq 4 \times 10^4$), the normalized radius of the lowest eigenmodes is $\rho_{e,0} \approx 3$, and Eq. 5 for this range reads

$$I_{ch} = 2 \times 10^{18} \frac{\eta_{ch}}{\lambda^2} \text{ W/cm}^2 \quad [7]$$

with λ given in units of micrometers.

It follows from the definition of N_{cr} that I_{ch} can be written in the form

$$I_{ch} = \frac{4\pi}{\rho_{e,0}} \frac{N_e}{N_{cr}} P_{ch} \lambda^{-2} = \frac{4\pi}{\rho_{e,0}} \frac{P_{ch}}{P_0} \frac{N_e}{N_{cr}} P_0 \lambda^{-2}. \quad [8]$$

Because both $\rho_{e,0}$ and P_{ch}/P_0 vary slowly over the range $10 \leq \eta_{ch} \leq 10^4$ ($\rho_{e,0} \approx \text{const}$, $P_{ch}/P_0 \approx \text{const}$), the peak intensity in the channel scales as

$$I_{ch} \sim \frac{N_e}{N_{cr}} P_0 \lambda^{-2}, \quad [9]$$

a result, which gives for a constant ratio of N_e/N_{cr} the simple scaling

$$I_{ch} \sim P_0 \lambda^{-2}. \quad [10]$$

From the obvious relation $N_e \approx \lambda^{-2}$ for $N_e/N_{cr} \cong \text{const}$, together with Eqs. 4 and 10, we conclude that at a constant ratio of N_e/N_{cr} the power density P/V is expected to vary as

$$P/V \sim P_0 \lambda^{-4}. \quad [11]$$

Within a margin of ≈ 10 percent, the results of our computations conform to this strong expected scaling favoring the UV.

In conclusion, detailed studies of the stability of relativistic/charge-displacement self-channeling have revealed two chief characteristics of this nonlinear mechanism of propagation: a dominant role for the lowest eigenmode for pulses launched in the stable zone and an exceptional robustness of the stability of single channels. As a consequence, strongly azimuthally perturbed incident intensity profiles can undergo efficient confinement to stable channeled distributions. The results demonstrate how a simple gradient in the electron density can be used to augment the effectiveness of the stable region and extend the channeling process into a high power-density regime that unites high propagating intensities with high plasma densities.

Support for this research was provided under contracts with the Strategic Defense Initiative/Naval Research Laboratory (N00014-93-K-2004), the Army Research Office (DAAH04-94-G-0089 and DAAG55-97-1-0310), the Department of Energy at the Sandia National Laboratories (DE-AC04-94AL85000), the University of California/Lawrence Livermore National Laboratory (B328353), and the Japanese Ministry of Education, Science, Sport, and Culture (08405009 and 08750046).

1. Borisov, A. B., Shiryayev, O. B., McPherson, A., Boyer, K. & Rhodes, C. K. (1995) *Plasma Phys. Control. Fusion* **37**, 569–597.
2. Borisov, A. B., Borovskiy, A. V., Korobkin, V. V., Prokhorov, A. M., Shiryayev, O. B., Shi, X. M., Luk, T. S., McPherson, A., Solem, J. C., Boyer, K. & Rhodes, C. K. (1992) *Phys. Rev. Lett.* **68**, 2309–2312.
3. Borisov, A. B., Shi, X. M., Karpov, V. B., Korobkin, V. V., Shiryayev, O. B., Solem, J. C., McPherson, A., Boyer, K. & Rhodes, C. K. (1994) *J. Opt. Soc. Am. B* **11**, 1941–1947.
4. Borisov, A. B., McPherson, A., Thompson, B. D., Boyer, K. & Rhodes, C. K. (1995) *J. Phys. B* **28**, 2143–2158.
5. Monot, P., Auguste, T., Gibbon, P., Jakobov, F., Mainfray, G., Dulieu, A., Louis-Jacquet, M., Malka, G. & Miquel, J. L. (1995) *Phys. Rev. Lett.* **74**, 2953–2956.
6. Young, P. E., Ford, M. E., Hammer, J. H., Kruer, W. L., Tabak, M. & Wilks, S. C. (1995) *Phys. Rev. Lett.* **75**, 1082–1085.
7. Wagner, R., Chen, S.-Y., Maksimchuk, A. & Umstadter, D. (1997) *Phys. Rev. Lett.* **78**, 3125–3128.
8. Borghesi, M., MacKinnon, A. J., Barringer, L., Gaillard, R., Gizzi, L. A., Meyer, C., Willi, O., Pukhov, A. & Meyer-ter-Vehn, J. (1997) *Phys. Rev. Lett.* **78**, 879–882.
9. Malka, G., Fuchs, J., Amiranoff, F., Baton, S. D., Gaillard, R., Miquel, J. L., Pépin, H., Rousseaux, C., Bonnaud, G., Busquet, M. & Lours, L. (1997) *Phys. Rev. Lett.* **79**, 2053–2056.
10. Sun, G.-Z., Ott, E., Lee, Y. C. & Guzdar, P. (1987) *Phys. Fluids* **20**, 526–532.
11. Borisov, A. B., Borovskiy, A. V., Korobkin, V. V., Prokhorov, A. M., Shiryayev, O. B. & Rhodes, C. K. (1990) *Phys. Rev. Lett.* **65**, 1753–1756.

12. Borisov, A. B., Borovskiy, A. V., Shiryaev, O. B., Korobkin, V. V., Prokhorov, A. M., Solem, J. C., Luk, T. S., Boyer, K. & Rhodes, C. K. (1992) *Phys. Rev. A* **45**, 5830–5845.
13. Pukhov, A. & Meyer-ter-Vehn, J. (1996) *Phys. Rev. Lett.* **76**, 3975–3978.
14. Sprangle, P., Esarey, E. & Hafizi, B. (1997) *Phys. Rev. Lett.* **79**, 1046–1049.
15. Pukhov, A. & Meyer-ter-Vehn, J. (1997) *Phys. Rev. Lett.* **79**, 2686–2689.
16. Borisov, A. B., McPherson, A., Thompson, B. D., Boyer, K. & Rhodes, C. K. (1997) in *Multiphoton Processes 1996: Proceedings of 7th International Conference on Multiphoton Processes*, eds. Lambropoulos, P. & Walther, H. (IOP, Bristol), Inst. Phys. Conf. Ser. No. 154, pp. 1–9.
17. McPherson, A., Cobble, J., Borisov, A. B., Thompson, B. D., Omenetto, F., Boyer, K. & Rhodes, C. K. (1997) *J. Phys. B* **30**, L767–L775.
18. McPherson, A., Thompson, B. D., Borisov, A. B., Boyer, K. & Rhodes, C. K. (1994) *Nature (London)* **370**, 631–634.
19. Bouma, B., Luk, T. S., Boyer, K. & Rhodes, C. K. (1993) *J. Opt. Soc. Am. B* **10**, 1180–1184.
20. Borisov, A. B., McPherson, A., Boyer, K. & Rhodes, C. K. (1996) *Progr. Crystal Growth Character. Mat.* **33**, 217–223.
21. Chiao, R. Y., Garmire, E. & Townes, C. H. (1964) *Phys. Rev. Lett.* **13**, 479–482.
22. Forslund, D. W., Kindel, J. M. & Lindman, E. L. (1975) *Phys. Fluids* **18**, 1002–1016.
23. Decker, C. D., Mori, W. B., Katsouleas, T. & Hinkel, D. E. (1996) *Phys. Plasmas* **3**, 1360–1372.
24. McPherson, A., Borisov, A. B., Boyer, K. & Rhodes, C. K. (1996) *J. Phys. B* **29**, L291–L297.
25. Bespalov, V. I. & Talanov, V. I. (1966) *J. Exp. Theor. Phys. Lett.* **3**, 307–309.
26. Campillo, A. J., Shapiro, S. L. & Suydam, B. R. (1973) *Appl. Phys. Lett.* **23**, 628–630.
27. Boyer, K., Jara, H., Luk, T. S., McIntyre, I. A., McPherson, A., Rosman, R. & Rhodes, C. K. (1987) *Rev. Phys. Appl.* **22**, 1793–1799.
28. Boyer, K. & Rhodes, C. K. (1985) *Phys. Rev. Lett.* **54**, 1490–1493.
29. Briggs, J. S. & Taulbjerg, K. (1978) in *Structure and Collisions of Ions and Atoms*, ed. Sellin, I. A. (Springer, Berlin), pp. 105–153.
30. Borisov, A. B., McPherson, A., Boyer, K. & Rhodes, C. K. (1996) *J. Phys. B* **29**, L113–L118.
31. Borisov, A. B., McPherson, A., Boyer, K. & Rhodes, C. K. (1996) *J. Phys. B* **29**, L43–L50.
32. Augst, S., Strickland, D., Meyerhofer, D. D., Chin, S. L. & Eberly, J. H. (1989) *Phys. Rev. Lett.* **63**, 2212–2215.

External Distribution:

Professor Charles K. Rhodes
University of Illinois-Chicago, Dept. of Physics
Rm. 2236
845 W. Taylor Street
Chicago, IL 60607-7059

Internal Distribution:

10	MS 1188	Stewart M. Cameron, 9512
1	MS 1188	John S. Wagner, 9512
1	MS 1188	Roy Hamil, 9512
1	MS 1188	Ting Shan Luk, 9512 (contractor)
1	MS 1188	David E. Bliss, 9512
1	MS 1188	Richard Adams, 9512
1	MS 1194	Frank Camacho, 9573 (contractor)
1	MS 1190	Craig Olson,
1	MS 1194	Rick B. Spielman, 9573
1	MS 1187	Eugene McGuire, 9571
1	MS 1186	Stephen Slutz, 9533
1	MS 1186	Mary Ann Sweeney, 9502
1	MS 1194	Chris Deeney, 9573
1	MS 1186	Tom Mehlhorn, 9507
1	MS 1196	Ray Leeper, 9577
1	MS 1196	Gordon Chandler, 9577
1	MS 1196	Mark Derzon, 9577
1	MS 1187	Keith Matzen, 9571
1	MS 1191	Jeffrey Quintenz, 9502
1	MS 1153	Malcolm Buttram, 9330
1	MS 1190	Don Cook, 9500
1	MS 1165	Joseph Polito, 9300
1	MS 0151	Gerold Yonas
1	MS 9018	Central Technical Files, 8940-2
2	MS 0899	Technical Library, 4916
2	MS 0619	Review & Approval Desk, 15102 For DOE/OSTI
1	MS 0188	LDRD Office (Attn: Donna L. Chavez)